A retinal circuit that vetoes optokinetic responses to fast visual motion

Adam Mani, Xinzhu Yang, Tiffany Zhao, Megan L. Leyrer, Daniel Schreck,
David M. Berson
Department of Neuroscience, Brown University, Providence, RI, USA.

Abstract

Optokinetic nystagmus (OKN) complements the vestibulo-ocular reflex (VOR) to stabilize the retinal image during head rotation. OKN is driven by the ON direction-selective ganglion cells (ON DSGCs), a rare class of retinal output neuron that encodes both the direction and speed of global retinal slip. The cells and synaptic circuits that give ON DSGCs their directional tuning are well known, but those dictating their slow-speed preference (and thus OKN's) remain enigmatic. Here, we probe this circuit through patch recordings, functional imaging, genetic manipulation, and serial electron microscopic reconstruction in mouse retina. We confirm earlier evidence that feedforward glycinergic inhibition is the main suppressor of ON DSGC responses to fast motion and reveal a surprising source for this inhibition — the VGluT3 amacrine cell, a retinal interneuron that releases both glycine and glutamate, exciting some neurons and inhibiting others. We find that VGluT3 cells respond robustly to fast global motion and that their output reaches most RGC types, as well as a diverse group of amacrine and bipolar cells. They *enhance* the response of ON-OFF DSGCs to fast motion, while *suppressing* it in ON DSGCs. Together, our results identify

23 a novel role for VGluT3 cells, limiting the range of retinal slip speeds that drive image-
24 stabilizing eye movements. More broadly, they suggest VGluT3 cells shape the
25 response of many RGCs and amacrine cells to fast motion.
26

27 Introduction

28 Animals see better when their visual systems are supported by sensorimotor
29 networks for image stabilization. Stabilizing the image on the photoreceptor array
30 simplifies crucial visual computations, such as extracting weak, noisy signals or
31 distinguishing the motion of objects from retinal image motion resulting from the
32 observer's own eye, head, or body movements.
33

34 Image-stabilizing reflexes are extremely widespread among animals with image-
35 forming eyes. In vertebrates, rotation of the head triggers vestibular and visual
36 feedback signals to brainstem and cerebellum oculomotor networks which generate
37 eye counter-rotation to cancel the global drift of the retinal image (retinal slip). These
38 innate responses comprise the vestibulo-ocular reflex (VOR) and the optokinetic
39 reflex (OKR) [1–3]. Both produce nystagmus, in which slow image-stabilizing eye
40 movements are periodically interrupted by fast resets of gaze in the opposite
41 direction.
42

43 Vestibular and visual image-stabilizing reflexes complement one another in the
44 velocity domain. The VOR plays the primary image-stabilizing role during rapid
45 rotatory motion of the head. Canal signals are strong, driving a powerful VOR that

46 nulls most of the retinal image motion. The modest residual slip triggers the OKR. At
47 slow speeds, for which VOR gain is weak, OKR is the dominant stabilization
48 mechanism and the two reflexes sum to achieve nearly perfect stabilization over a
49 broad range of rotational speeds. The OKR is speed-tuned. It must be responsive to
50 slow slip velocities to compensate for the limitations of the VOR. but it must be
51 insensitive to fast speeds or it would thwart fast eye movements, such as saccades or
52 the fast resetting phase of nystagmus.
53
54 Among the more than three dozen types of mammalian retinal ganglion cells (RGCs)
55 [4–6], only a very specific subset appear to participate in visually driven image
56 stabilization. These are direction-selective ganglion cells (DSGCs), and mainly those of
57 a specific subclass – the ON DSGCs. They send their axons almost exclusively to the
58 nuclei of the accessory optic system (AOS) [1,2,7], which relays their retinal slip
59 signals to the vestibulocerebellum and through it to the oculomotor system. This
60 circuit, including apparently homologous ON DSGCs, is highly conserved across
61 vertebrates. The far more common ON-OFF class of DSGCs makes only a small
62 contribution to this circuit, projecting instead mainly to the lateral geniculate nucleus
63 and superior colliculus.
64
65 ON DSGCs, like the OKR they drive, respond best to slow speeds of retinal slip,
66 typically ~1°/s, depending on species and stimulus [2,8,9]. They are effectively silent
67 during fast visual motion, as during saccades or the fast phase of nystagmus. By
68 contrast, ON-OFF DSGCs respond well to such fast motion [9] (but see [10]). Other

69 types of RGCs exhibit diverse speed tuning profiles, with some highly responsive to
70 very fast motion.
71
72 ON DSGCs thus encode both components of the vector of retinal slip used by the
73 image-stabilization system – its speed and direction. The mechanisms conferring
74 direction selectivity on these and other DSGCs, anchored by starburst amacrine cells
75 (SACs), have been studied in great detail [11–14]. By contrast, much less is
76 understood about the cell types, neurotransmitters, and synaptic circuits that confer
77 slow speed tuning upon ON DSGCs or distinct speed-tuning profiles upon other RGC
78 types.
79
80 Diverse mechanisms may underlie slow-speed tuning in ON DSGCs. Excitatory drive
81 might be attenuated at higher speeds due to suboptimal spatiotemporal summation of
82 excitatory inputs across the dendritic arbor [15] or intrinsic membrane properties
83 that filter out the high-frequency excitatory currents induced by fast motion.
84 Alternatively, fast motion might trigger presynaptic inhibition of the bipolar cells (and
85 VGluT3 amacrine cells [16]) which provide excitatory input to ON DSGCs.
86
87 In an alternative candidate mechanism, amacrine cells activated by fast global retinal
88 slip would provide direct feedforward inhibition onto the ON DSGC. A study in rabbit
89 retina showed that just such a circuit confers slow speed tuning on ON DSGCs, and
90 demonstrated that the inhibitory transmitter is glycine [9]. The closely related
91 ON-OFF DSGCs lack this glycinergic input and respond well to fast speeds [9].

Here in mouse retina we have used serial block face electron microscopy (SEM), patch recordings, and cell-type-specific optogenetics and chemogenetics to delineate the synaptic networks responsible for vetoing ON DSGC responses at high speeds. Our observations in mice echo the rabbit findings: direct feedforward glycinergic inhibition of ON DSGCs is primarily responsible [9] for their slow speed preference. We next exploit connectomics to identify an unexpected source of this glycinergic inhibition — the VGluT3 amacrine cell — an unusual amacrine cell that makes excitatory (glutamatergic) synapses onto some postsynaptic targets and inhibitory (glycinergic) synapses onto others [17–19]. A prior optogenetic study found an excitatory glutamatergic VGluT3 input to ON DSGCs [16]. Though we replicate that result in a few ON DSGCs, the dominant synaptic influence is glycinergic inhibition. We demonstrate that this provides the main basis for vetoing the ON DSGCs response to fast global retinal slip.

Previous studies have shown that VGluT3 cells have strong receptive-field surrounds [16,20], which would seem incompatible with robust responses to fast global motion. However, our calcium imaging data demonstrate robust activation of VGluT3 dendrites by global motion, weakened surrounds when the stimulus is moving, and a marked preference for fast motion.

We confirm that the other major class of DSGCs, the ON-OFF DSGCs — receive only excitatory glutamatergic input from VGluT3 cells. This *augments* their responses to

115 fast motion, in contrast to the suppressive influence in ON DSGCs. The connectomic
116 data document widespread VGluT3 output to most types of RGCs. This suggests that
117 these amacrine cells may play a major role in sculpting the retinal output during fast
118 motion, by enhancing the responses of some RGCs and inhibiting others. In ON DSGCs,
119 it vetoes the response of the image-stabilization system to fast velocities such as those
120 generated by gaze shifts, neatly separating these two visuo-oculomotor realms.
121

122 **Results**

123 ***Inhibition at fast speeds underlies slow speed tuning in mouse ON DSGCs.***
124 To explore the speed-tuning mechanism, we made patch recordings of synaptic
125 currents and spiking responses in ON DSGC during presentation of full-field gratings
126 drifting in the preferred direction at various speeds. We located these rare RGCs using
127 2-photon imaging of fluorescent reporters (Hoxd10-GFP or Pcdh9-Cre) or by
128 surveying extracellular spike responses of RGCs of intermediate size for characteristic
129 responses to flashed stimuli (see Supplemental Information and Methods). In all
130 cases, we confirmed the identity of ON DSGCs from their selectivity for the direction of
131 grating drift and through dye-filling and imaging of their characteristic dendritic
132 morphology (see Supplemental Information and Supp. Fig. S1).
133

134 As expected, ON DSGCs were remarkable among RGCs in preferring slower speeds of
135 grating drift (Fig. 1A-C, blue curves). Optimal spiking responses were obtained at
136 retinal speeds of 150 ± 11 μm/s (angular velocity of 5 ± 2°/s; mean ± SEM; n = 63),
137 close to previously reported values for mouse ON-DSGCs and OKN gain [2]. This is

138 probably a slight overestimate of preferred speed; about one in four cells responded
139 best to the slowest speed tested (76 μm/s) and thus may have preferred even slower
140 speeds. Spike responses were strongly attenuated at speeds above the optimum,
141 dropping to half their maximum spike rate at roughly twice the optimum speed (360
142 ± 23 μm/s, 12 ± 0.8°/s). Many other RGC types responded to much higher speeds of
143 grating drift (Fig. 1C). For example, ON-OFF DSGCs exhibited optimum speeds about
144 four times faster than those of ON DSGCs (600 ± 70 μm/s; half max. speeds 2000 ±
145 160 μm/s, 67 ± 5 °/s, (n = 17), Fig. 1C). Some RGC types responded to even higher
146 speeds. For example, ON alpha cells maintained better than half-maximal responses
147 even above 3000 μm/s (100 °/s) . Other RGC types, such as ON-delayed RGCs [21],
148 shared the slow speed tuning of ON DSGCs.
149
150 We hypothesized that the preference of mouse ON-DSGCs for slow speeds would
151 result from direct glycinergic inhibition, as demonstrated in rabbit retina [9]. To test
152 this idea, we first used whole-cell voltage clamp to record excitatory and inhibitory
153 currents evoked in ON DSGCs by various speeds of grating drift in the preferred
154 direction (Fig. 1A,B, red, orange curves). Both excitatory and inhibitory input were
155 broadly tuned for speed, but with different profiles. Excitation was present at the
156 slowest speeds we tested, but rose with speed, peaking at speeds five times faster
157 than those evoking the most robust spiking (710 ± 90 μm/s (n = 11), or 24 °/s).
158 Excitation declined to half its maximum at 2290 ± 170 μm/s. Thus, although
159 excitatory drive is affected by speed, this is insufficient to explain the slow speed
160 tuning in ON DSGCs.

161

162 Though inhibition was strongest at speeds close to those evoking the strongest
163 excitation (1220 ± 170 μm/s, declining half max. > 2900 μm/s, n = 12), it was
164 relatively weaker than excitation at slow speeds and relatively stronger at fast ones.
165 The crossover of the two curves occurred at ~700 μm/s, above which nearly all
166 spiking was suppressed (Fig. 1A). Taken together, the above results imply that slow
167 speed tuning of ON DSGCs reflects a shift in excitatory-inhibitory balance in favor of
168 inhibition at higher speeds, as in the rabbit [9].

169

170 For most speeds, the excitatory current traces exhibited a single prominent peak for
171 each cycle of the grating (Fig. 1B), presumably reflecting glutamatergic input from ON
172 bipolar cells, their dominant source of excitation. In contrast, inhibitory current traces
173 often exhibited minor peaks roughly anti-phase to the excitation, when the dark bars
174 of the grating overlie the receptive field. The OFF pathway may therefore make a
175 larger contribution to inhibition than to excitation. At higher speeds, the inhibitory
176 current exhibited not only the stimulus-locked modulatory component but also an
177 underlying continuous inhibitory conductance. This was much less apparent for
178 excitation. This confirms earlier observations in rabbit ON DSGCs.

179

180 ***Fast retinal slip triggers feedforward glycinergic inhibition of ON DSGCs***

181 We repeated these experiments adding receptor antagonists to the bath to test the
182 hypothesis that the feed-forward inhibition evoked at fast speeds was glycine-
183 mediated, as in rabbit (Fig. 1D,E). The glycine receptor antagonist strychnine sharply

184 attenuated the inhibition, dramatically reducing the steady plateau of inhibition
185 evoked by fast grating motion. At speeds evoking maximum inhibitory current, total
186 inhibition was reduced by more than half its control value (57±4% decrease in charge
187 transfer; n=3. See note in Supplemental Information). In contrast, blockade of $GABA_A$
188 receptors alone (SR95531) had only a modest effect (Fig. 1D,E; 17±7% decrease in
189 charge transfer; n=3). Simultaneous application of both antagonists abolished all
190 inhibitory current in the ON DSGCs. Thus, effectively all inhibition driven by fast
191 motion is mediated by $GABA_A$ and glycine receptors under our experimental
192 conditions.
193
194 Taken together, these results demonstrate that fast motion triggers direct glycinergic
195 inhibition of ON DSGCs, as first shown in rabbit [9]
196
197
198
199
200

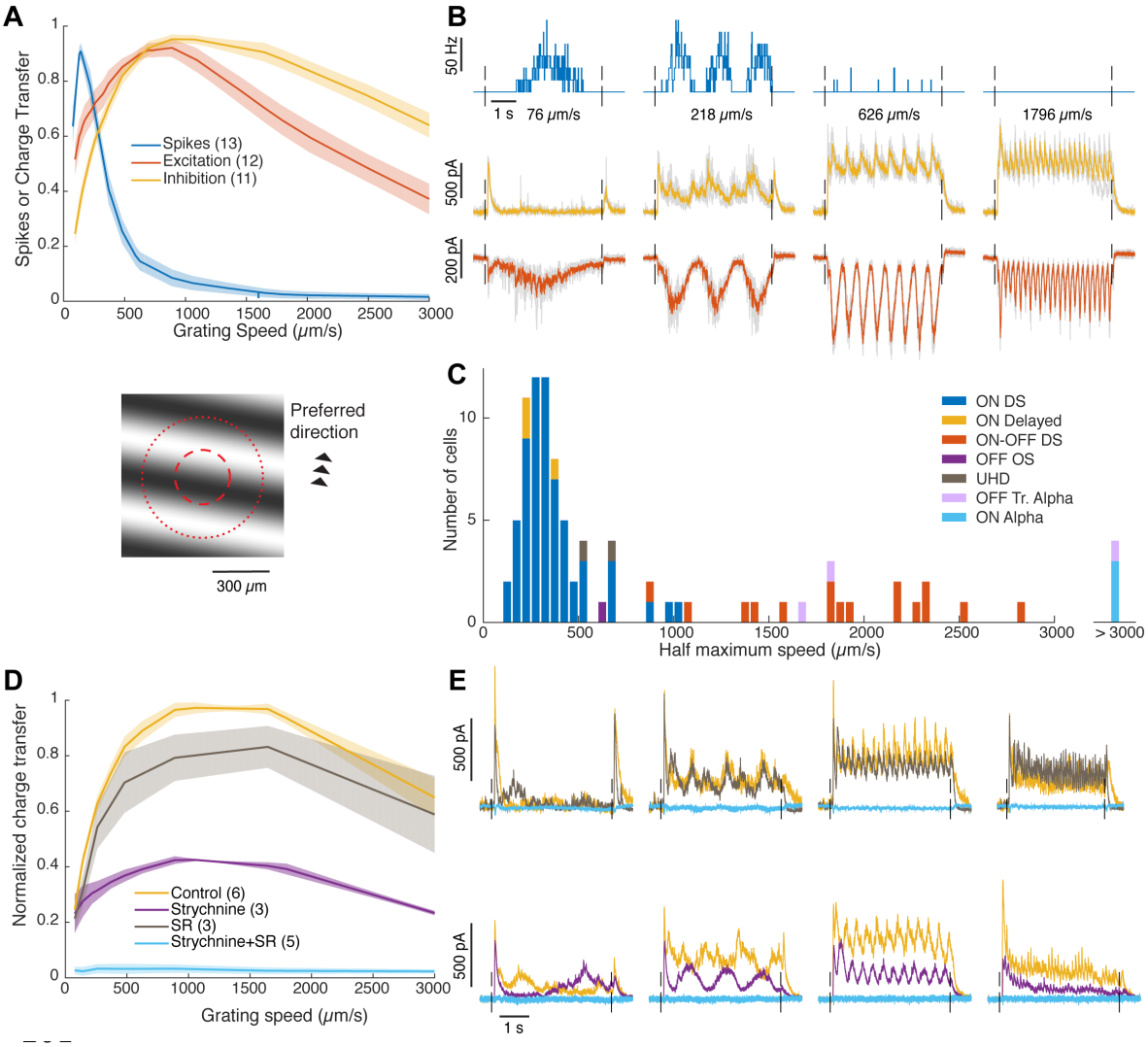

Figure 1. Inhibitory mechanism underlying slow speed tuning in ON DSGCs. , (A) Top: Speed tuning in the response of ON DSGCs to moving gratings, as revealed by spiking (blue) and synaptic currents (excitation: red; inhibition: orange). Curves are population averages; all are normalized to their maxima. Shading denotes standard error of the mean (S.E.M.). Currents, expressed as charge transfer, were measured at a holding voltage of -65 mV (excitation) and +20 mV (inhibition). Bottom: the grating stimulus shown to scale with a schematic ON DSGC receptive field (center and surround; red circles). (B) Time course of mean spiking and current responses (±S.E.M.) to different grating speeds; color scheme as in A. (C) Distribution of speed preferences among RGCs of different functional types as indexed by the highest speed capable of evoking a response half that evoked by the optimal speed. (D) Pharmacological analysis of the inhibitory conductance. Selective glycinergic blockade (purple; strychnine) strongly reduces the inhibition seen under control conditions (orange), while blocking ionotropic GABA receptors (black; SR95531) had a weaker effect. Combined application (blue) blocked all inhibition. (E) Effects of GABA blockade (black; top row) or glycinergic blockade (purple; bottom row) on the time course of inhibitory currents. In both cases, the other antagonist was subsequently added to the first, blocking all inhibition (blue).

218 ***Electron microscopic reconstructions identify VGluT3 amacrine cells as the***
219 ***primary source of glycinergic synapses onto ON DSGCs.***
220 Most glycinergic retinal inhibition derives from small-field amacrine cells with highly
221 branched dendritic arbors [22,23]. We searched for synaptic contacts from such cells
222 onto ON DSGCs in an existing serial blockface electron microscopic (SEM) dataset of
223 the adult mouse inner plexiform layer spanning >200 μm (volume 'k0725' [24]). We
224 focused our analysis mainly on a single previously reconstructed presumed ON DSGC
225 (Fig. 2) [15]. Numerous anatomical features identify this as an ON DSGC. Its dendrites
226 narrowly costratify with the processes of starburst amacrine cells (SACs), with nearly
227 the entire arbor within the ON SAC plexus (Fig. 2B-E). There, they cofasciculate with
228 SAC processes (Fig. 2A) and receive numerous wrap-around synaptic contacts [12]
229 from SAC varicosities (Fig. 2F, G). Analysis of the orientation of the presynaptic SAC
230 processes confirmed the asymmetric connectivity that confers direction selectivity
231 upon DSGCs [12–15]. The minor OFF branches, a common feature of ON DSGC arbors
232 in mice [2], receive some OFF SAC contacts. Presumptive ON-OFF DSGCs in the volume
233 shared many of these attributes but had smaller dendritic arbors, higher branching
234 density, and a larger fraction of their arbor in the OFF SAC plexus.
235

236 To identify possible sources of glycinergic amacrine cell inhibition to this ON DSGC,
237 we first marked all the non-ribbon synaptic contacts we could find (n=431; Fig. 2F-I).
238 For each contact, we reconstructed enough of the presynaptic process to sort it into
239 one of three groups (Fig. 2A-E): SACs; wide-field amacrine cells; or candidate
240 glycinergic neurons. SACs were recognizable from their narrow stratification within

241 the ON or OFF SAC plexus, thin straight connecting dendrites, and large wrap-around
242 varicosities targeting mainly other SACs and DSGCs. Wide-field cells had sparser
243 branching and fewer varicosities and were not strictly confined to the SAC plexuses.
244 Candidate glycinergic neurons were much more highly branched, with arbors that
245 extended well outside the SAC plexuses.

246

247 SAC inputs accounted for fully 83% of the non-ribbon contacts (n=340; 317 ON and
248 23 OFF). At least by this measure, GABAergic SAC input dominates the inhibition of
249 ON DSGCs. Candidate glycinergic inputs (n=41) were the next most common,
250 comprising 10% of non-ribbon inputs, with wide-field inputs nearly as common at 7%
251 of all input (n=27). A small minority of inputs (n=23; 5%) could not be identified
252 because too small a fraction of the arbor could be reconstructed, and were excluded
253 from the sample.

254

255 We extensively reconstructed all of the presumptive glycinergic neurons identified by
256 our initial screen. To our surprise, nearly all of them appeared to be VGluT3 amacrine
257 cells, as documented below (n=38 synapses from 16 cells). Two were synapses from
258 Type H18 amacrine cells [25,26] and one was from an unidentified medium-field type.
259 We detected no synaptic inputs from any of the many other types of small-field
260 amacrine cell types, even after examining a large sample of such cells reconstructed in

261 another study [26]. We conclude that VGluT3 amacrine cells are by far the best
262 candidate glycinergic cell type shaping the slow-speed tuning of ON DSGCs.
263
264 Multiple structural observations confirm these as VGluT3 amacrine cells (Fig. 3). First,
265 their stratification is appropriate (Fig. 3E, F, J). They arborize most heavily in the
266 middle of the inner plexiform layer (IPL), between the ON and OFF SAC plexuses, but
267 extend sparse processes into and even a bit beyond those plexuses . Their cell bodies
268 lie in the inner nuclear layer, are of appropriate size, and are distributed with spacing
269 that suggests a regular mosaic (Fig. 3A). Their dendritic-field diameters (106 ± 7 μm,
270 n = 10 cells) are in line with earlier data [18,20] and overlap extensively with a
271 coverage factor of at least 5 (Fig. 3A, inset).
272
273 Input and output patterns matched previous reports on VGluT3 cells, and were very
274 consistent across the population of reconstructed cells (Fig 3I, Supplemental Table
275 S5), confirming other evidence that they belong to a single type. In keeping with
276 functional evidence for input from both the ON and OFF pathways to VGluT3 cells, our
277 reconstructed cells receive ribbon synapses from diverse ON and OFF bipolar cells.
278 The complement of bipolar inputs largely reflects their dendritic stratification (Fig.
279 3G, I) with most input from OFF types 3a, 3b, and 4 and ON types 5o, 5i, 5t, and little
280 from bipolar types stratifying at the IPL margins (OFF types 1,2 and GluMI [27]), and
281 ON types 6, 7, 8 and 9. Their outputs include all the ganglion-cell targets so far
282 identified in physiological studies (Supplemental Table S5). These included W3 cells
283 [16,28], OFF transient alpha cells [29], Suppressed-by-Contrast cells of several types

284 [29,30] including the ON Delayed RGC [21] (see Discussion), both ON and ON-OFF
285 DSGCs [16,28], and M1 ipRGCs [31] (For RGC type nomenclature see [4] and
286 accompanying online database). However, our SEM analysis suggests that their
287 outputs are much more diverse than previously appreciated, with contacts to the
288 great majority of known RGC types [4], including OFF sustained alpha , Jam-B [32], ON
289 alpha, F-mini-ON [33], F-mini-OFF [33], OFF transient medium RF, and diverse
290 varieties of smaller field RGCs stratifying between the ChAT bands [34]. Two ipRGC
291 types notably not targeted by VGluT3 are the M2 [35] and M5 (PixON) [36,37] types,
292 which stratify largely outside the VGluT3 plexus. VGluT3 cells also synapsed upon
293 diverse types of amacrine cells, though only rarely onto other VGluT3 cells or SACs.
294 We have not reconstructed most amacrine-cell targets, though WF cells stratifying
295 between the SAC plexuses were among the most common recipients [38]. VGluT3
296 outputs, like their ribbon inputs, were distributed most heavily within and between
297 the SAC plexuses (Fig. 3H), though they were also sparsely present in the distal IPL.
298 Some of these are somato-dendritic synapses onto M1 ipRGCs. One unexpected
299 feature of the VGluT3 cells in this volume was a consistent upward (roughly dorsal)
300 displacement of the dendritic arbor relative to the soma (Fig. 3B-D).

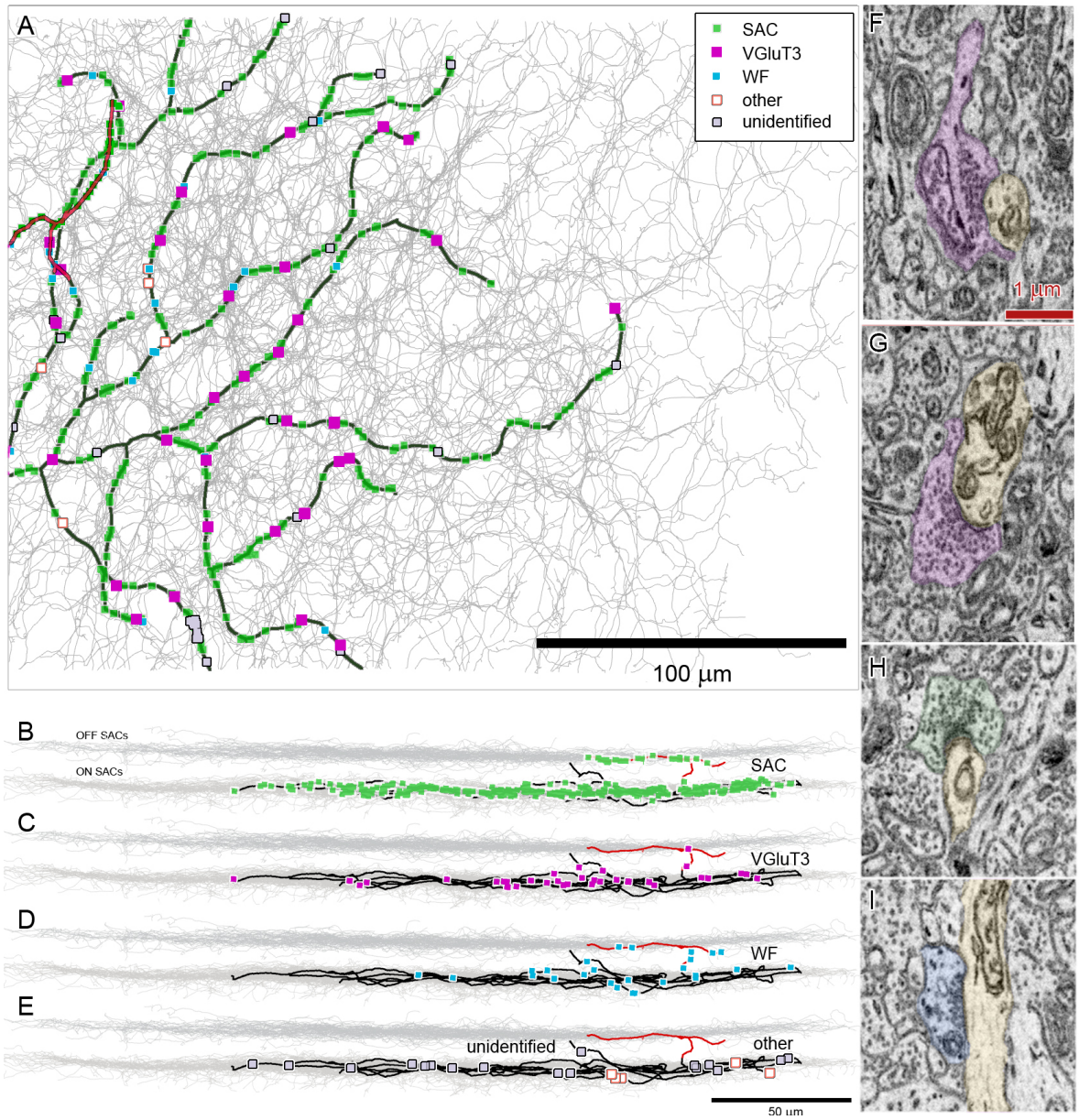

Figure 2. Amacrine cell inputs onto an ON DSGC. (A) SEM reconstruction of the distribution and sources of all detected amacrine-cell synaptic contacts onto an ON DSGC. Dendrites of the ganglion cell are shown in black except for the sparse branches in the OFF sublayer (red). Synaptic contacts are plotted as dots, color coded by amacrine-cell source (see key), as determined by reconstruction of presynaptic cells. The plexus of ON SAC dendrites is shown in gray. Boundaries of the SEM volume appear as a fine rectangle. (B-E) side (vertical) views of depth of these inputs within the IPL. Gray bands mark the ON and OFF SAC plexuses. (G-I) Example SEM images of amacrine-cell synapses onto the ON DSGC. The ON-DSGC is shown in yellow. The presynaptic cells are color coded as in A-E: VGluT3 cells (F,G), an ON SAC (H) and a WF amacrine cell (I).

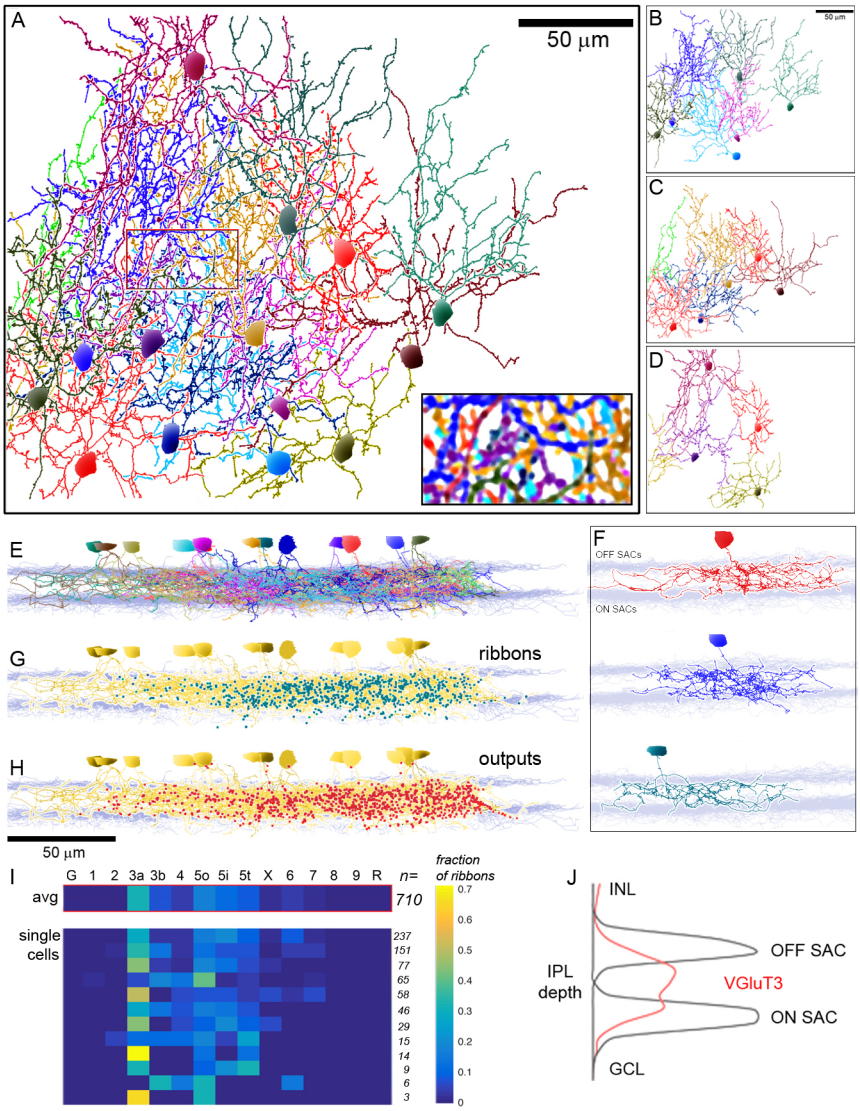

Figure 3 Morphology, input and output of VGluT3 amacrine cells. (A-D). Dendritic arbors and mosaic of VGluT3 amacrine cells reconstructed in the k0725 SEM volume as seen in top view (*en face*). Enlarged view (inset) shows that local regions contain dendrites of at least 5 VGluT3 cells. B-D: Same dendritic profiles as in A but divided arbitrarily into three groups to provide a clearer view of single arbors. (E,F) Side (vertical) views of the stratification of reconstructed VGluT3 cells within the IPL, shown together (E) and, for 3 cells, individually (F). (G, H) Side view of the location in depth of ribbon inputs (F) and synaptic outputs (G) of VGluT3 cells. Gray bands in E-H mark the ON and OFF SAC plexuses; VGluT3 cells appear gold in G and H. (I) Heatmap plot of the fraction of all ribbon synaptic inputs derived from each bipolar type, identified at the top (G – GluMI, X – XBC, R – rod bipolar cell). Bar at top shows pooled data for all identified ribbon contacts (n=710). Lower panel illustrates the consistency of this pattern across individual cells, shown one per row in descending order of the number of identified ribbons. (J) Stratification profile of reconstructed VGluT3 processes (red; n=17) in relation to those of ON and OFF SACs (black). Data are normalized to the ON SAC plexus.

329 ***VGluT3 cells make functional glycinergic synapses onto ON DSGCs***

330 Of the three types of amacrine cells shown by the SEM analysis to provide input to ON
331 DSGCs, only one – the VGluT3 cell – is known to be glycinergic. Thus, VGluT3 cells are
332 apparently the source of most, if not all, the glycinergic suppression of ON DSGCs
333 during rapid motion. The other two presynaptic types – SAC and widefield amacrine
334 cells – use GABA as their sole inhibitory transmitter [23,39–41]. This is a surprising
335 conclusion because VGluT3 ACs have been reported to provide glutamatergic
336 excitation to ON DSGCs, not glycinergic inhibition [16]. To test for the inferred
337 glycinergic influence, we recorded postsynaptic currents evoked in ON DSGCs by
338 optogenetic depolarization of VGluT3 cells. For these studies, we crossed a novel
339 strain of VGluT3-Cre mice with a strain that expresses channelrhodopsin2 (ChR2) in a
340 Cre-dependent manner (Ai32) (See Methods and Supplemental Information, Supp.
341 Fig. S2). Conventional photoreceptor-mediated light responses and cholinergic
342 transmission were suppressed with a cocktail of synaptic blockers ('photoreceptor
343 block'; L-AP4, ACET, hexamethonium [16]). Optogenetic activation of VGluT3 cells
344 evoked robust inhibitory currents in 81% of the ON DSGCs tested (13/16 cells) (Fig.
345 4A-C). Peak inhibitory postsynaptic currents averaged 33 ± 4 pA for single light
346 pulses. We also delivered optogenetic pulse trains to mimic the temporal modulation
347 of VGluT3 cells during grating motion (Fig. 4D). Evoked inhibitory currents persisted
348 in postsynaptic ON DSGCs throughout a 5 s train over the full range of frequencies
349 tested (1-8 Hz, corresponding to grating speeds of roughly 400 - 3000 μm/s for
350 experiments shown in Fig. 1). At higher stimulus frequencies, IPSCs summed
351 temporally to produce a continuous inhibitory conductance (Fig. 4D bottom traces),

352 much as they did during rapid grating motion (Fig. 1B, yellow traces). Thus, inhibition
353 of ON DGSCs by VGluT3 cells exhibits kinetics compatible with their proposed role in
354 vetoing responses to fast motion.
355
356 The inhibition evoked by activation of VGluT3 cells was glycinergic, as expected.
357 Blocking ionotropic glutamate receptors (CNQX, D-AP5) had little effect on the
358 optogenetically induced inhibitory conductance (Fig 4A, B; mean reduction in
359 maximal current of 28 ± 7%, 5 cells), whereas further blockade of glycine receptors
360 (strychnine) virtually eliminated the current (decrease of 81 ± 5%, 4 cells). The
361 broad-spectrum glutamate blockade used ensures that these photostimulation-
362 induced currents are mediated optogenetically, not because rods and cones are
363 driving glutamatergic signals through synaptic networks. It also excludes indirect
364 effects mediated by evoked release of glutamate from VGluT3 cells. We conclude that
365 these amacrine cells inhibit ON DSGCs through direct glycinergic synaptic input.
366
367 We reversed the order of drug application in three cells. When strychnine was the
368 first inhibitory blocker applied, the optogenetically evoked inhibition was completely
369 suppressed in one cell (Fig 4C, left). However, in two other cells, strychnine left at
370 least half the inhibition intact. This residual inhibition was abolished upon further
371 addition of the glutamate receptor antagonists (Fig 4C, right). Presumably this
372 strychnine-resistant inhibitory current occurs when VGluT3 activation
373 glutamatergically excites one or more GABAergic amacrine cell types that synapse
374 onto ON DSGCs (see Discussion).

375

376 Control experiments confirmed that off-target ChR2 expression in Müller cells was not
377 responsible for the evoked currents in ON DSGCs; that other known targets of VGluT3
378 input responded as expected to the optogenetic stimulus (Fig. 4E); and that the
379 pharmacological effects shown in Fig. 4B,C were not simply the result of rundown of
380 optogenetic responses over trials (Supplemental Information, Supp. Fig. S3).

381

382 To evaluate a previous report that VGluT3 cells provide glutamatergic excitation to
383 ON DSGCs [16], rather than glycinergic inhibition as found here, we repeated these
384 experiments with ON DSGCs clamped at the chloride reversal potential.
385 Optogenetically evoked EPSCs were detected in only two of the 16 cells tested (12%),
386 with peak currents of 10 ± 1 pA (Fig. 4F, G). The excitation was mediated by
387 glutamate: it persisted following application of strychnine, but was eliminated by
388 application of the ionotropic glutamate receptor blockade (Fig. 4G). Both of those cells
389 also exhibited evoked IPSCs when clamped at 0 mV.

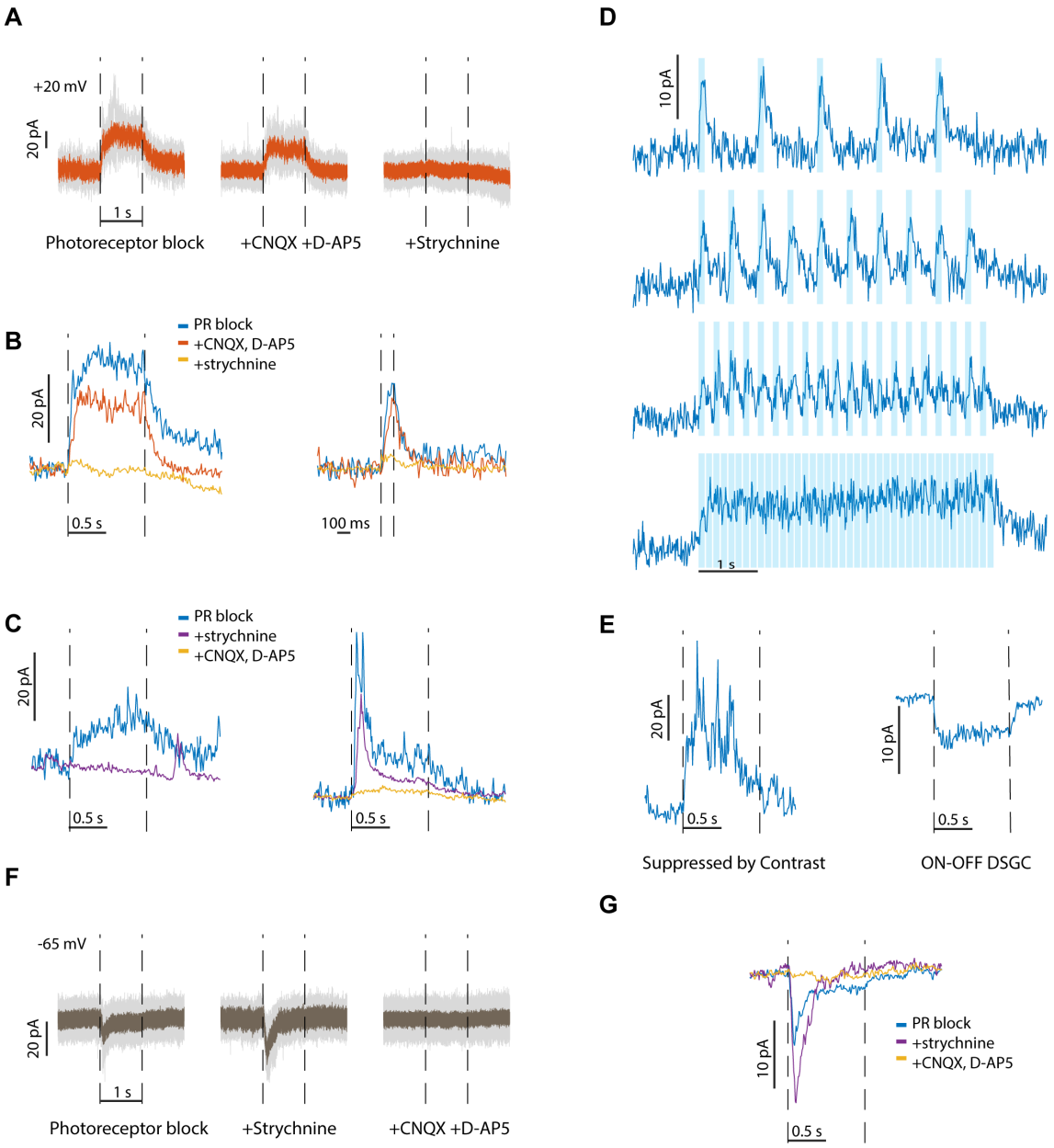

Figure 4. Postsynaptic currents evoked in ON DSGCs by optogenetic activation of VGluT3 cells. (A) Raw inhibitory current trace (V_{hold}: +20 mV) in a single ON DSGC in response to optogenetic stimulation during the period marked by interrupted vertical lines. "Photoreceptor block" consists of L-AP4, ACET and Hexamethonium. (B) Pharmacological effects on the evoked inhibitory current in two ON DSGCs (left and right panels; left panel from same cell as in A). The sequence of drug application is listed above; current traces are smoothed. (C) As for B, but with glycinergic blockade preceding glutamatergic blockade. (D) Inhibitory currents in an ON DSGCs in response to optogenetic pulse trains of frequencies 1, 2, 4, 8 Hz. Pulse width: 100 ms. (E) Optogenetic activation of VGluT3 cells evokes inhibitory currents in a Suppressed by Contrast RGC (V_{hold}: +20 mV), and excitatory currents in an ON-OFF DSGC (V_{hold}: -65 mV; both under photoreceptor block). (F) Excitatory currents (raw) evoked in an

402 ON DSGC by optogenetic activation of VGluT3 cells. V_{hold}: -65 mV. (G) Pharmacological effects on this
403 current in the same cell.
404

405

406 ***Chemogenetic suppression of VGluT3 cells reduces fast-motion inhibition of ON***
407 ***DSGCs***

408 We tested the effects of chemogenetically suppressing VGluT3 cells on the inhibition
409 of ON DSGCs by fast motion. We used a DREADD system (Designer Receptor
410 Exclusively Activated By Designer Drugs) in VGluT3-Cre mice, expressing the hM4Di
411 receptor in VGluT3 cells either by intraocular injection of a Cre-dependent viral vector
412 or by crossing VGluT3-Cre mice with Cre-dependent DREADD mice (Methods). In
413 either case, bath-application of the DREADD ligand (CNO) markedly reduced the
414 inhibitory currents induced by drifting gratings at all speeds (Fig. 5A, B). At speeds
415 evoking maximal inhibition, CNO reduced inhibitory charge transfer by 43 ± 7% (n =
416 3) for viral experiments and 38 ± 6% (n = 3) for those based on the genetic cross. The
417 same ligand had no effect on inhibition in an ON DSGC in a DREADD-free mouse (Fig.
418 5C).
419

420 The chemogenetic approach (Fig. 5A, B) was less effective than strychnine (Fig. 1D) in
421 reducing the motion-induced inhibition in ON DSGCs. Indeed, addition of strychnine
422 during the chemogenetic manipulation further reduced the inhibition (Fig. 5D, E).
423 This could reflect incomplete chemogenetic suppression of VGluT3 output or
424 alternative sources of glycinergic inhibition beyond VGluT3 cells. Application of CNO
425 scaled down the currents by about the same factor across speeds (Fig 5A, B, E) while

426 preserving the kinetics (Fig. 5E), which is consistent with incomplete suppression of
427 VGluT3 (see Supplemental Information and Discussion).
428
429 Taken together, the above results suggest that the native inhibition in ON DSGCs at
430 high speeds is provided at least to a large extent by glycine release from VGluT3 cells,
431 although our effort to suppress VGluT3 signaling was only partially effective.
432
433 ***VGluT3 cells augment fast-motion responses in ON-OFF DSGCs***
434 We found that the other direction-selective class, the ON-OFF DSGCs, were excited by
435 optogenetic activation of VGluT3 cells excites (Fig.4E), in agreement with earlier work
436 [16,28]. Thus, VGluT3 cells appear to exert essentially opposite signs of effect on the
437 two DSGC classes. ON-OFF DSGCs responded well to fast gratings that induced strong
438 glycinergic suppression in ON DSGCs (Fig. 5F, 1C). This suggested that glutamate
439 release from VGluT3 cells may augment ON-OFF DSGC responses in this range of
440 speeds. Indeed, chemogenetic suppression of VGluT3 cells reduced the excitation
441 evoked in ON-OFF DSGCs by fast gratings moving in the preferred direction (17 ± 3%
442 reduction in excitatory charge transfer from its control value; Fig. 5G). The reduction
443 was more pronounced at faster speeds: the speed response curves (Fig. 5G) were
444 shifted towards lower speeds at the falling branch (Δ = 400 ± 160 μm/s at half max. of
445 the control curves). Though incomplete blockade of VGluT3 cells may underrepresent
446 these influences, most of the residual excitatory current presumably represents
447 bipolar ribbon synaptic input. Thus, during rapid visual motion, VGluT3 cells affect

the two DSGC classes in opposing ways, enhancing responses in ON-OFF DSGCs while suppressing ON DSGCs.

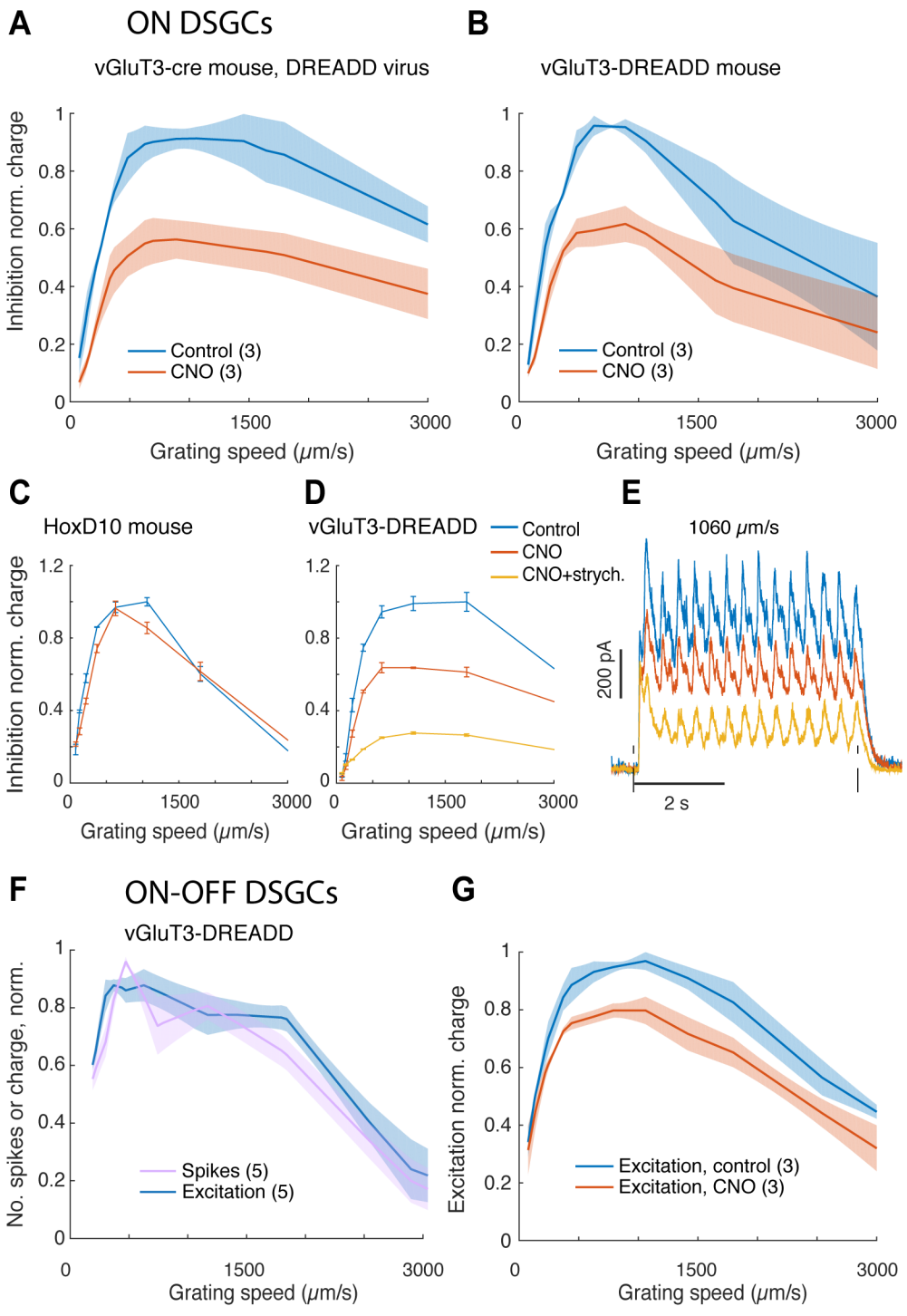

452 **Figure 5. Chemogenetic suppression of VGluT3 cells alters speed tuning of ON and ON-OFF**
453 **DSGCs.** Effect of DREADD-mediated suppression of VGluT3 cells on speed tuning in ON DSGCs (A-E)
454 and in ON-OFF DSGCs (F,G). (A, B) Application of the DREADD ligand CNO (red trace) partially
455 suppressed inhibitory currents evoked by moving gratings in ON DSGCs under control conditions
456 (blue), regardless of whether the method for Cre-dependent DREADD expression was intraocular
457 injection of a Cre-dependent virus (A) or through a genetic cross (B). V_{hold} : +20 mV. (C) Control
458 experiment showing that CNO has no effect when applied in a DREADD-free retina from a HoxD10-GFP
459 mouse. (D) Most inhibition that remains after CNO application is blocked by further addition of the
460 glycine-receptor antagonist strychnine.-(E) Individual current traces of the ON DSGC in D under the
461 same pharmacological conditions and using the same color scheme as in D. Grating speed: 1060 μm/s.
462 (F) Spiking and synaptic excitation in ON-OFF DSGCs as a function of grating speed. V_{hold} : -65 mV (G)
463 Speed tuning profiles of excitatory charge in ON-OFF DSGCs , before and after application of CNO. For
464 experiments in F and G, DREADD was expressed through a genetic cross.
465
466

467 ***VGluT3 dendrites are strongly activated by fast global motion***

468 The foregoing results imply that fast motion triggers VGluT3 output. To provide more
469 direct evidence on this point, we recorded their calcium responses using GCaMP6
470 expressed selectively in these cells using a genetic cross (VGluT3-Cre x Ai148) [42].
471
472 VGluT3 dendrites exhibited robust calcium signals in response to the motion of full-
473 field grating stimuli, especially at the fast speeds that trigger feedforward glycinergic
474 inhibition of ON DSGCs. Speed tuning was highly consistent for different ROIs within
475 each field of view, and across most fields of view (FOV; Fig. 6C), and at different
476 depths within the VGluT3 plexus. Some FOVs exhibited an unusually robust response
477 to the fastest speeds (Fig. 6C, right panel).
478
479 The robust response to extended stimuli was unexpected because VGluT3 receptive
480 fields have strong suppressive surrounds [16,20,42]. Indeed, calcium responses were
481 greatly enhanced when we restricted the same gratings to a circular patch centered

482 on the FOV (345 μm diam.; Fig. 6D). This enhancement was apparent at all speeds, and
483 quadrupled the response to the optimal speed. Slow gratings that failed to drive
484 responses when presented full-field now evoked clear Ca^{2+} signals. Nonetheless, the
485 high-speed preference remained.
486
487 To probe the spatial organization of these surround effects, we presented spots or
488 masked gratings of various sizes centered on the FOV (Fig. 6E,F). Area-response
489 profiles based on spot stimuli closely resembled those reported earlier based on patch
490 recordings from VGluT3 somas [20](Fig. 6E; green curve), with strong surround
491 suppression and maximal responses for spots ~200 μm in diameter (ON response:
492 204 ±10 μm; 20 ROIs. OFF response: 217±12 μm; 19 ROIs). Grating patches (blue
493 curve) produced a markedly different area-response profile, with much less response
494 attenuation as grating patches extended into the surround. For the largest stimuli
495 tested (930 μm diam.) grating responses persisted about a quarter of their maximum
496 response (26 ± 3%, 28 ROIs), whereas spot responses were suppressed to less than a
497 tenth of their maximum (ON: 8 ± 1%, 20 ROIs; OFF 4 ± 1%, 19 ROIs). Further, when
498 gratings were used, the optimum size of the stimulus was roughly doubled (408 ± 10
499 μm; 28 ROIs). We conclude that though VGluT3 cells have strong receptive-field
500 surrounds, the surround suppression is stimulus-dependent and permits robust
501 responses to global retinal motion.
502
503 The difference in surround suppression between the two stimuli (Fig. 6E) could arise
504 from the presence or absence of continuous motion. Alternatively it could be the

505 result of a contrast increase during the stimulus time. The spot stimulus by its nature
506 is a step in overall contrast (positive or negative) with respect to the preceding and
507 surrounding background. The gratings however, were presented on a gray
508 background, with the mean change in overall contrast being zero. We thus tested new
509 sets of spots and gratings, with overall contrast in the two stimuli equal and positive
510 (Fig. 6F; see Methods). The area-response functions for spots resembled those seen
511 previously (Fig. 6E), though the lower contrast weakened the responses. The
512 surround suppression for masked gratings, however, was stronger than for zero mean
513 gratings. Despite this, receptive fields sizes assessed with gratings were once again
514 larger than those measured with spots of equal contrast (Fig. 6F). Therefore, the
515 weaker surround suppression in the case of gratings vs. spots, is both due to a smaller
516 change in contrast, and due to the continuous motion.
517
518 Taken together our results suggest that VGluT3 ACs are fit to report global image slip
519 and do not exhibit a prohibitive surround suppression.
520
521 To our surprise, the VGluT3 dendritic Ca^{2+} signals were tuned to the direction of
522 grating motion. (Fig. 6G, H). Typically, individual ROIs exhibited a preference for
523 grating motion in either direction along a single axis; 84% of ROIs met the standard
524 criterion for this form of orientation selectivity (OS; 69 of 82 ROIs, 5 FOVs, 3 mice).
525 Many ROIs preferred motion in one direction; 57% met the standard criterion for
526 direction selectivity (DS, 47 ROIs). Only 5% (4 ROIs) showed neither orientation or
527 direction preference (43% met both criteria). In some FOVs, ROIs were either mostly

528 orientation selective (Fig. 6G, top) or mostly direction selective (Fig 6G, middle), while
529 other FOVs contained a mix of OS and DS behavior (Fig 6G, bottom). Overall OS ROIs
530 (69) were strongly clustered around a preference for dorsoventral axis of motion
531 (~70° or 250°); a minor second cluster appeared near the nasotemporal axis (~20° or
532 200°) (Fig. 6I, left). Preferred directions of DS ROIs (47) clustered mainly near the
533 nasotemporal axis (~200°). Note that we defined the preferred orientation as the
534 preferred axis of motion (not e.g. as the orientation of the bars in the grating).
535

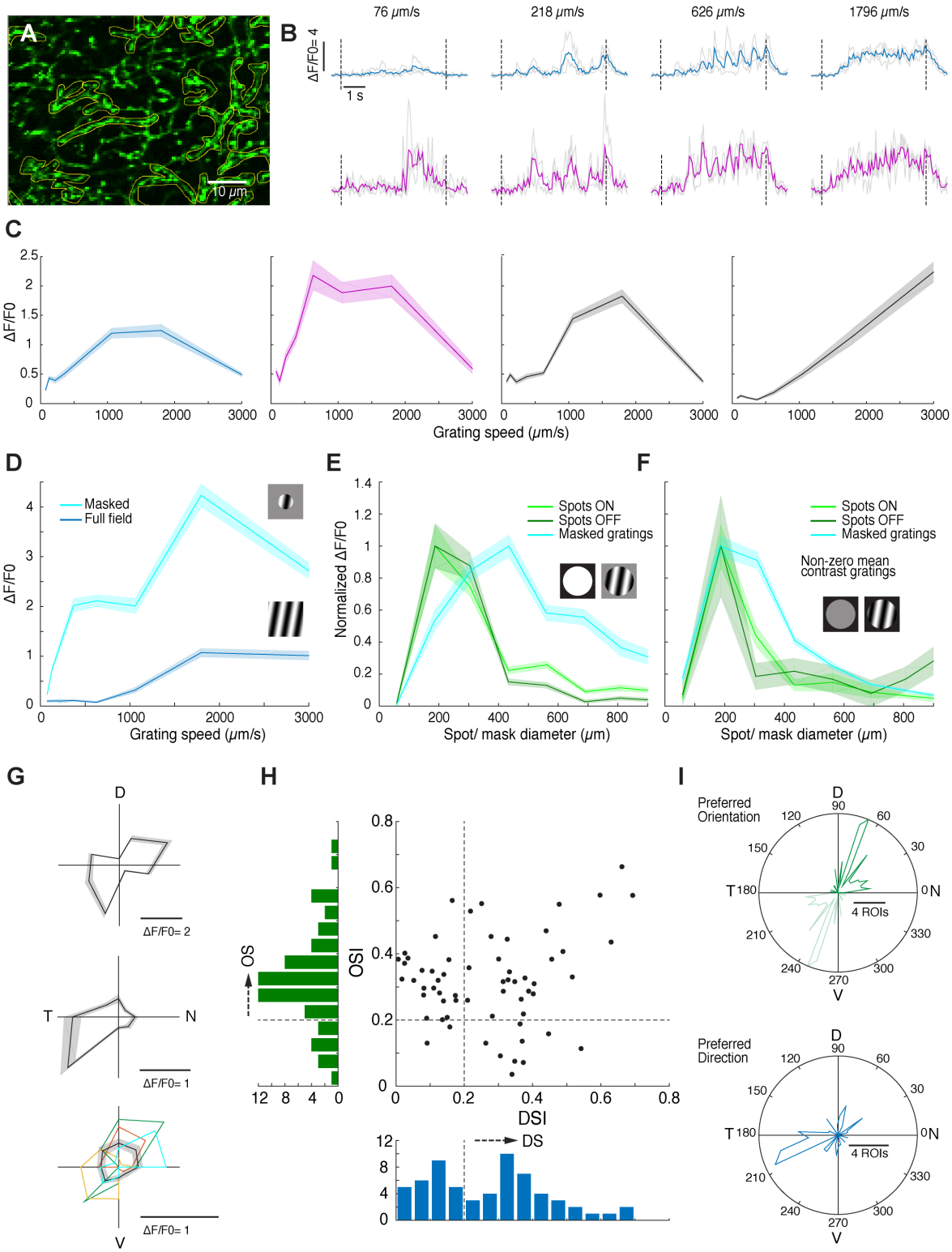

Figure 6. Calcium responses in VGluT3 AC dendrites. (A) Part of a field of view of a live flat-mounted retina at the level of the VGluT3 dendritic plexus, marked by GCaMP6 fluorescence. Yellow outlines show typical ROIs used to assess local Ca^{2+} signals. (B) Temporal variation in fluorescence intensity ($\Delta F/F_0$) in two ROIs (top and bottom rows), in response to full-field gratings drifting in one

direction at different speeds, noted above the traces. Individual trials, gray; mean over trials, blue or magenta. (C) Net calcium response ($\Delta F/F_0$, averaged over the stimulus time) to full-field gratings as function of speed for four different FOVs; data for all ROIs in the field were pooled. The two left panels (blue and magenta) include data from the ROIs of the corresponding color in B. (D) As for C, but varying the extent of the grating to assess surround suppression of the grating response. Responses are greatly enhanced when the grating moves within a circular mask (345 μm diameter). (E) Area-response functions for flashed bright spots presented from darkness (green traces) and for drifting gratings (blue trace). Spot responses are shown separately for the ON (light green) and OFF responses (dark green). For gratings, size tuning was assessed by presentation within a circular mask of variable size (speed: 1520 μm/s; direction fixed but chosen arbitrarily, presented from gray background). (F) Same as in E., but the spots and gratings are matched in net positive contrast relative to the background. (G-I) Evidence for orientation and direction selectivity of the VGluT3 dendritic plexus. (G) Polar plots of average responses vs. the direction of motion of a full-field grating (speeds 1500 or 1900 μm/s) in 3 FOVs. Colored curves in bottom panel show data for several individual ROIs. (H) Distributions of orientation and direction selectivity indices (OSI and DSI) of 63 ROIs, 3 FOVs shown in G. An ROI was considered DS or OS if its DSI or OSI was ≥ 0.2, respectively. (I) Angular distributions of the preferred orientations (top), or preferred directions of (bottom) of single ROIS (n= 69 OS ROIs and 47 DS from 5 FOVs).

Discussion

Optokinetic image stabilization is triggered by slow image drifts but not by fast retinal motion such as occurs during saccades. Here, we identify the inhibitory synaptic circuit primarily responsible for this speed selectivity in mice. It features a familiar amacrine cell type - the VGluT3 cell - in a surprising new role. We show that VGluT3 cells respond well to fast global motion, and that they veto ON DSGC responses to fast motion through feedforward glycinergic inhibition.

Our conclusions are supported by a wealth of convergent evidence. Our pharmacological findings recapitulate earlier evidence in rabbit implicating glycinergic inhibition as the key suppressor of fast motion responses in ON DSGCs. Connectomic analysis shows that just three types of amacrine cells account for nearly

574 all conventional (non-ribbon) synaptic contacts onto ON DSGCs, only one of which -
575 the VGluT3 cell - is glycinergic. We show that the VGluT3 plexus is strongly activated
576 by rapid motion, and that this is true even during global retinal slip, despite the strong
577 suppressive surrounds of VGluT3 receptive fields. We confirm that optogenetic
578 activation of VGluT3 cells evokes glycinergic inhibitory currents in ON DSGCs whereas
579 chemogenetic suppression of VGluT3 output reduces the inhibition of ON DSGCs
580 triggered by rapid motion. Though our data points to feedforward glycinergic
581 inhibition from VGluT3 cells as the main determinant of slow speed preference in ON
582 DSGCs, their speed-tuning profile is undoubtedly shaped to some extent also by their
583 excitatory inputs [15] and by their GABAergic inputs from SACs and widefield
584 amacrine cells.
585
586 The output of ON DSGCs to the accessory optic system encodes the local vector of
587 global retinal slip, a precondition for proper image stabilization during head rotation.
588 The vector has two components: direction and speed. The directional coding is well
589 known to derive mainly from a specific amacrine-cell type, the SAC, through spatially
590 asymmetric feedforward GABAergic inhibition of the ON DSGC. We argue that the
591 other vector component is supplied by synaptic input from VGluT3 amacrine cells.
592 These dual-transmitter interneurons excite some RGCs through glutamate release,
593 while inhibiting others through glycine. An earlier pair of studies reported only
594 excitatory glutamatergic transmission from VGluT3 cells to ON DSGCs [16], not
595 glycinergic inhibition [29]. Though we confirmed some VGluT3-mediated
596 glutamatergic excitation of ON DSGCs, it was present only in a minority of cells and

597 was weaker and more sustained than in the earlier findings. The difference may be
598 partly attributable to our 20-fold dimmer photostimulation stimulus. As far as we are
599 aware, this is the first time any neuronal type has been shown to receive both
600 excitatory and inhibitory input from VGluT3 cells. SACs are also dual-transmitter
601 amacrine cells, exciting DSGCs through nicotinic receptors as well as inhibiting them
602 through GABA. Together, SACs and VGluT3 cells account for more than 92% of the
603 total inhibitory synapses onto ON DSGCs, as shown by our reconstructions. The
604 remaining inhibitory inputs come almost entirely from widefield amacrine cells.
605
606 Image stabilization is ubiquitous among animals and crucial for effective vision during
607 self-motion. Optokinetic and optomotor responses are present in all major vertebrate
608 classes and always exhibit preferential activation by slow retinal slip. Many of the
609 genes, cell types, and brain pathways that support such image-stabilizing reflexes are
610 likewise highly conserved in mammals and other vertebrates. Both SACs and VGluT3
611 cells have been described in higher primate retinas [43–45], so the same two cell
612 types may encode the two components of the global retinal slip vector in the human
613 retina as they do in mice. Genetic defects perturbing this circuit disrupt normal image
614 stabilization in human patients [3].
615
616 *VGluT3 cells differentiate the functional signals of ON and ON-OFF DSGCs*
617 It has been known for half a century that ON DSGCs prefer slow speeds while ON-OFF
618 DSGCs prefer faster speeds [8]. The mechanistic basis of this difference has remained
619 obscure. In this report, we show that VGluT3 cells respond vigorously to rapid global

motion and use glycinergic feedforward inhibition to suppress ON DSGCs' response to fast motion. ON-OFF DSGCs, on the other hand, lack VGluT3 inhibition which presumably enables their fast-motion responses. However, VGluT3 cells further differentiate the speed preferences of the two DSGC classes by augmenting fast-motion responses in ON-OFF DSGCs though excitatory glutamatergic synapses.

The two classes of DSGCs have distinct functional roles. ON DSGCs are by far the dominant visual input to the accessory optic system and vestibulocerebellum, which convert slow retinal slip signals into slow optokinetic image-stabilizing eye movements. ON-OFF DSGCs direct their output instead to the superior colliculus and lateral geniculate nucleus, and thus on to the visual cortex. The collicular output allows object motion to trigger gaze or attentional shifts, while the cortical pathway exploits motion information for numerous perceptual computations including figure-ground segmentation, depth perception, and encoding of self-motion. A broad range of speeds are relevant to these midbrain and cortical functions, but for image stabilization, the key motion signal is slow global retinal slip. This specific spatiotemporal pattern of visual reafference informs the brain of a shortfall in the vestibular image-stabilizing reflex, the VOR. If this system were responsive to fast motion, it would conflict with the gaze-shifting network, because it would trigger image stabilization during the fast retinal slip produced by saccades. Silencing the image stabilization system at the retinal level, rather than in downstream brain networks, is energetically favorable since it achieves the same outcome with fewer spikes.

643

644 The differing requirements of these two systems in the speed domain is
645 accommodated by the differing speed-tuning profiles of the two classes of DSGCs (ON
646 vs ON-OFF). Our findings now allow us to trace this functional difference back one
647 step further to VGluT3 cells, a interneuron with robust fast-motion-responses and
648 opposing transmitter actions on the two classes: glycinergic inhibition of ON DSGCs,
649 and glutamatergic excitation of ON-OFF DSGCs.

650

651 *Are VGluT3 cells the sole source of glycinergic inhibition of ON DSGCs?*
652 Strychnine effectively blocks all glycine receptors on ON DSGCs as shown by the
653 observation that all residual motion-induced inhibition is eliminated by blocking
654 GABA receptors (Fig. 1D). Chemogenetic suppression of VGluT3 cells selectively was
655 less effective in eliminating this feedforward glycinergic inhibition since adding
656 strychnine further reduced it. This may indicate that there are other sources of
657 glycinergic input. The connectomic analysis did identify two synapses from H18
658 amacrine cells [25,46] to ON DSGCs. If H18 cells are glycinergic, as suggested by their
659 relatively small, highly branched dendritic arbors, their contributions to ON DSGC
660 inhibition would have been blocked by strychnine but not by our chemogenetic
661 manipulation. However, the transmitter composition of H18 cells is unknown, and
662 they synapse onto ON DSGCs only very rarely. We therefore favor an alternate
663 explanation - that VGluT3 cells are virtually the sole glycinergic input, but that our
664 chemogenetic manipulation of them was only partly effective. This could have
665 occurred for several reasons. When the exogenous receptor was expressed virally,

666 some fraction of VGluT3 cells may not have been transduced. Even when the receptor
667 was presumably expressed ubiquitously through a Cre-dependent genetic cross,
668 application of CNO failed to block the inhibition as completely as strychnine did. This
669 might indicate that the inhibitory K^+ current evoked by activation of the designer
670 receptor was too weak to suppress all light-evoked synaptic release from VGluT3
671 terminals. A scaling down of VGluT3 output of this sort could account for the finding
672 that the CNO-sensitive inhibition was a fixed fraction of the total strychnine-sensitive
673 inhibition across the full range of speeds, and that the shapes of the inhibitory current
674 traces were preserved following CNO application (Fig. 5A, B, Supplemental
675 Information and Fig. S4). The alternative model, in which the chemogenetic silencing
676 of VGluT3 cells is incomplete, cannot easily account for such a simple scaling-down of
677 the glycinergic inhibition because the postulated alternative source of inhibition
678 would have to closely match VGluT3 cells in speed tuning. These two models are not
679 exhaustive; others mechanisms might account for the discrepancy between the
680 chemogenetic and strychnine effects. For example, because strychnine blocks glycine
681 receptors globally, it might alter the inhibition measured in ON DSGCs indirectly by its
682 impact on other synaptic circuits.
683
684 *New insights into VGluT3 connectivity and function*
685 The synaptic machinery supporting dual glycine/glutamate transmission from
686 VGluT3 cells to their postsynaptic partners remains opaque. The two transmitters
687 could be co-released at the same active zone, with the sign of effect determined
688 mainly by postsynaptic receptor composition. Alternatively, there could be spatially

689 segregated sites of glycine and glutamate release. Our SEM reconstructions provide
690 the first opportunity to compare the ultrastructure of VGluT3 output synapses known
691 to be functionally glycinergic or glutamatergic. Contacts onto known targets of the
692 glutamatergic output (ON-OFF DS; OFF transient alpha; W3/UHD cells) were
693 conventional contacts, not ribbon synapses. Nor were they obviously different in size
694 or form from synapses onto targets known or shown here to be predominantly
695 inhibitory (Suppressed-by-Contrast cells of various forms [29,30,47], ipRGCs [31] and
696 ON DSGCs (present study). Of course, a closer examination or better ultrastructural
697 data might reveal such differences.
698
699 The connectomic evidence suggests that the direct influences of VGluT3 cells extend
700 far more widely to other retinal neurons than appreciated in earlier functional
701 surveys. They encompass diverse RGCs and amacrine cells as well as some cone
702 bipolar cells. Other VGluT3 cells are rarely the target of synaptic output from this
703 amacrine cell type, which stands in marked contrast to the extensive mutual
704 inhibition between SACs.
705
706 In the absence of obvious ultrastructural correlates of the two sorts of VGluT3 output
707 synapses, we cannot infer whether the previously unknown output targets receive
708 glutamatergic or glycinergic influence from VGluT3 cells. However, our study does
709 offer one small clue. In the presence of glycinergic blockade, optogenetic activation of
710 VGlut3 cells evoked a presumptive GABA-mediated inhibitory current in some ON
711 DSGCs. This suggests that that VGluT3 cells supply glutamatergic excitation to one or

712 both of the GABAergic amacrine cell types that synapse onto ON DSGCs. One of these
713 types, the SACs exhibits no synaptic currents in response to optogenetic activation of
714 VGluT3 cells [16], nor did our SEM analysis turn up more than a very few synaptic
715 contacts from VGluT3 cells to SACs. This leaves the widefield amacrine cells as the
716 likely conduit for this influence. Whatever the circuit responsible, this indirect
717 influence of VGluT3 cells is net inhibitory onto the ON DSGC, just as the direct
718 glycinergic influence is.
719
720 Since SEM analysis implied that virtually all types of RGCs receive some VGluT3 input,
721 the role identified here for VGluT3 cells in sculpting the speed-tuning profiles of
722 DSGCs (both ON and ON-OFF) is likely to extend broadly to the retinal output. For RGC
723 types getting excitatory glutamatergic drive from VGluT3 cells, we would expect
724 boosted sensitivity to relatively fast motion. OFF transient alpha cells are one such
725 type and our data confirm their high-speed sensitivity. When the VGluT3 contribution
726 is inhibitory, we expect it to favor responses to slow speeds in the postsynaptic
727 ganglion cells, as for ON DSGCs. Just such a functional influence seems to be detectable
728 in a bistratified medium-field RGC type variously termed ON-delayed [21],
729 Suppressed by Contrast [30,47,48], R-cell [49], or Type 73 [6]. They are ON-type
730 RGCs, but their spiking response to light steps exhibits a characteristic delay which
731 was traced in part to fast feedforward glycinergic inhibition [21]. Ostensibly the same
732 type was inhibited by optogenetic activation of VGluT3 cells [30], and we confirm the
733 synaptic contacts from VGluT3 cells onto this type by SEM. Taken together, these
734 findings imply that this cell type might, like the ON DSGCs, prefer slow speeds. Our

735 survey of speed tuning of various RGC types appears to confirm this (Fig. 1C), since
736 ON-delayed cells were the only RGC type to prefer speeds as slow as those preferred
737 by ON DSGCs.
738
739 *The surprising responsiveness of VGluT3 cells to global motion*
740 Ca^{2+} imaging revealed robust responses to global motion in VGluT3 dendrites. This is
741 unexpected because VGluT3 cells are known to be strongly suppressed by visual
742 stimulation of their receptive-fields surrounds [16,20,42]. Responsiveness to global
743 motion also seems at odds with the reported selectivity of these cells for local object
744 motion [20,42]. We have shown that the strength of surround suppression is context
745 dependent, as is often the case [50,51]. When the receptive field is probed with a
746 moving grating of various sizes, rather than with flashed spots, the surround appears
747 weaker and the center appears larger ([16], Fig. 6E, F). For gratings instead of spots,
748 both motion and the lack of a sudden and sustained contrast step led to a weaker
749 surround suppression. During retinal slip of a natural visual image, no sudden
750 appearance or large changes in contrast occur, and thus VGluT3 surround
751 suppression should be minimal.
752
753 Though we have highlighted here the responsiveness of VGluT3 cells to global motion,
754 they may nonetheless participate in object-motion sensing, as proposed in relation to
755 their glutamatergic excitation of W3 RGCs [20,42]. Indeed gratings localized to a patch
756 resulted in much stronger responses in VGluT3 dendrites than full-field ones (Fig 6D).
757 The complete suppression measured previously for global motion could well be due

758 to the use of a different stimulus than ours, and specifically the stimulus duration:
759 these studies tested the responses to a short uniform motion of the grating (a 100 μm
760 translation during 0.25-0.5 s). An initial delay in the response relative to the stimulus
761 onset can be seen in our fluorescence traces as well (Fig. 6B) although it could be
762 attributable to voltage-calcium dynamics. Other stimulus parameters (e.g. grating
763 cycle length, orientation, relatively slow speed) could also have an effect.
764
765 *Sensitivity of VGluT3 cells to the axis or direction of movement*
766 Virtually every patch of the VGluT3 plexus we tested (95%) showed selectivity for
767 either the axis (orientation) or the direction of grating motion. This was unexpected,
768 and reveals yet another striking parallel with the SACs, whose dendrites are also
769 direction selective. There are also striking differences between the two types in this
770 regard. Though single SAC dendrites prefer somatofugal motion, SAC dendrites of
771 diverse orientations and directional preferences are intermixed at any location in the
772 dendritic plexus, and pooled local Ca^{2+} responses reveal no obvious directional bias at
773 the population level [24]. The VGluT3 plexus, however, shows strong biases in the
774 pooled local signal. An unresolved question is how the directional or orientation
775 preference differs, if at all, between neighboring VGluT3 cells, or within the arbor of a
776 single cell.
777
778 If VGluT3 dendrites are orientation/direction selective, can they still suppress fast-
779 motion responses in all four cardinal directions, and thus in all four ON DSGC
780 subtypes? We suggest they do: VGluT3 directional preference exhibited considerable

781 local variability, even when the net preference was strongly skewed. Preferences
782 differed even more across FOVs. Since ON DSGCs have very large dendritic arbors
783 (~10-12 times larger than the FOV area), they presumably sum inhibition from
784 VGluT3 cells spanning a large region and diverse preferences. Still, the observed bias
785 in VGluT3 motion preferences suggest possible interactions in the optokinetic system
786 between the direction and speed of retinal slip; ON DSGC subtypes preferring some
787 directions may be more strongly suppressed by fast speeds than others.
788
789 The connectivity of VGluT3 cells to nearly all RGC types means that their
790 contributions to shaping RGC response properties may extend beyond speed tuning to
791 include selectivity for the direction or axis (orientation) of motion. It will be of
792 interest to assess whether VGluT3 tuning for orientation and direction are linked to
793 their own dendritic asymmetry (as revealed at least in this volume; Fig. 3A-D),
794 similarly to the asymmetric arbors in two RGC types: the ON-OFF DSGCs preferring
795 ventral motion [52] and of JamB-OFF orientation-selective cells [53].
796

797 **Methods**

798 *Animals.* All procedures were in accordance with the National Institutes of Health
799 guidelines and approved by the Institutional Animal Care and Use Committee at
800 Brown University. Detailed below are the strains of mice used, of adult mice of either
801 sex, 2–8 months old. Wildtype C57BL/6J (Jackson Laboratory); To target ON DSGCs
802 for recording, HoxD10-GFP (GENSAT collection, Tg(Hoxd10-
803 EGFP)LT174Gsat/Mmucd, MMRRC #032065) and Pcdh9-Cre (GENSAT collection,

804 Tg(Pcdh9-Cre)NP276Gsat/Mmucd, MMRRC #036084) were used. The VGluT3-Cre
805 line (The Jackson Laboratory, B6;129S-*Slc17a8*$^{tm1.1(cre)Hze}$/J, #028534) was crossed
806 with Ai32 (Jackson, B6.Cg-*Gt(ROSA)26Sor*$^{tm32(CAG-COP4*H134R/EYFP)Hze}$/J, #024109) for
807 optogenetics, DREADD (Jackson, B6.129-*Gt(ROSA)26Sor*$^{tm1(CAG-CHRM4*,-mCitrine)Ute}$/J,
808 #026219) for chemogenetics, Ai14 (Jackson, B6;129S6-*Gt(ROSA)26Sor*$^{tm14(CAG-}$
809 $^{tdTomato)Hze}$/J, #007908) for characterization of the VGluT3-Cre mouse, and Ai148
810 (Jackson, B6.Cg-*Igs7*$^{tm148.1(tetO-GCaMP6f,CAG-tTA2)Hze}$/J, #030328) for Ca^{2+} imaging. For the
811 Müller cell control experiment, GLAST-Cre (Jackson, Tg(Slc1a3-cre/ERT)1Nat/J,
812 #012586) was crossed with Ai32.
813
814 *Retinal dissection.* Isolation of the retina was performed similarly to [54]. The eyes
815 were removed and immersed in oxygenated Ames medium (95% O2, 5% CO2; Sigma-
816 Aldrich; supplemented with 23 mM NaHCO3 and 10 mM d-glucose). Under dim red
817 light, the globe was cut, and cornea, lens and vitreous humour removed. A relieving
818 ventral cut was made in the eyecup, and the retina was isolated. three more cuts were
819 made in the retina, roughly along the temporal, nasal and dorso-nasal directions, the
820 asymmetry of which was used to disambiguate retinal orientation. The retina was flat-
821 mounted on a polylysine coverslip (Corning, #354086), which was secured in a
822 recording chamber.
823
824 *Tamoxifen injections.* Tamoxifen (Sigma-Aldrich) was dissolved in corn oil (Sigma-
825 Aldrich) to make 20 mg/ml, sonicated (30 minutes, RT) and placed in hot water (2
826 hrs, 45 °C) and once homogenous, filtered in a 0.2 μm filter. Tamoxifen was injected

827 IP, 2-2.5 mg per mouse, 3 days in a row. This resulted in dense YFP labeling of Müller
828 glia in GLAST-Cre x Ai32 mice [55]. The animals were used in experiments three
829 weeks after the last tamoxifen injection.
830
831 *Electrophysiology.* Patch-clamp recordings of isolated flat-mount retina were
832 performed under current-clamp using a Multiclamp 700B amplifier, Digidata 1550
833 digitizer, and pClamp 10.5 data acquisition software (Molecular Devices; 10 kHz
834 sampling). Pipettes were pulled from thick-walled borosilicate tubing (P-97, Sutter
835 Instruments). Retinas were continuously superfused during experiments with
836 oxygenated Ames' medium at 32 °C, flow rate ~5 ml/minute. For cell attached
837 recordings, Ames filled pipettes were used (tip resistance of 4-5 MΩ). For whole cell
838 voltage clamp recordings, pipettes filled with cesium internal solution (In mM: Cs
839 methane sulfonate, 104.7, TEA-Cl, 10, HEPES, 20, EGTA, 10, QX-314, 2, ATP-Mg, 5,
840 GTP-Tris, 0.5, pH 7.3, osmolarity 276 mOsm; All purchased from Sigma-Aldrich) were
841 used (tip resistance of 5.5-6.5MΩ). To isolate excitatory and inhibitory synaptic
842 currents, the recorded cell was held near the reversal potential for inhibition (~ -65
843 mV) and excitation (~ +20 mV), respectively. Application of synaptic blockers to the
844 bath as well as Clozapine-N-Oxide (CNO) was done by switching the perfused medium
845 into medium containing the blocker and waiting for ~7 minutes. The blockers used
846 were: strychnine (1 μM, Sigma), SR95531 (10 μM, Sigma), L-AP4 (20 μM, Tocris),
847 ACET (10 μM, Tocris), Hexamethonium (100 μM, Sigma) CNQX (20 μM, Tocris), D-AP5
848 (50 μM, Tocris). In the DREADD experiments, CNO was used to activate the DREADD
849 (1 nM, Sigma).

850

851 *Light stimulation.* Light stimuli were generated as in [54]. Patterned visual stimuli,
852 synthesized by custom software using Psychophysics Toolbox under Matlab (The
853 MathWorks), were projected (AX325AA, HP) and focused onto the photoreceptor
854 outer segments through the microscope's condenser. The projected display covered
855 ~1.5 × 1.5 mm (5.8 μm/pixel). The video projector was modified to use a single UV
856 LED lamp (NC4U134A, Nichia). The LED's peak wavelength (385 nm) shifted to 395
857 nm after transmission through a 440 nm short-pass dichroic filter (FF01-440/SP,
858 Semrock), a dichroic mirror (T425lpxr, Chroma), and various reflective neutral
859 density filters (Edmund Optics). The photoisomerization rates used were 10^2-10^3
860 R*/rod/s, and for the used spectrum were similar among rods, M-cones and S-cones.
861 In the beginning of a stimulus sequence, a uniform screen with the stimulus' mean
862 intensity (gray) was projected for 20-30s for light adaptation.
863 To identify RGC types, the spike responses of the cell to a 460 μm spot of +0.95
864 contrast were recorded. To assess the directional tuning of ON DSGCs we used a full-
865 field sinusoidal gratings (cycle = 377 μm, contrast = 0.95, stimulus duration = 5 s,
866 inter-stimulus duration = 3 s at uniform mean grating intensity) drifting in 8
867 directions in a randomized sequence (drift speed = 226μm/s, 4 repetitions). For
868 speed response curves, the same grating was drifted in the preferred direction
869 (DSGCs), at 7-8 different speeds at a randomized sequence, with 3 repetitions for each
870 speed. For VGluT3 dendrites Ca^{2+} imaging, the same stimulus was used, with the
871 direction of motion chosen arbitrarily. The same was also presented in a circular
872 patch on a gray background in Fig. 6D. In Fig 6E, white spots of different sizes were

873 presented from dark, and the grating stimulus was presented from gray in circular
874 masks of different sizes. In Fig. 6F, gratings and gray spots of different sizes (gray =
875 the mean intensity of the gratings) were both presented from dark, to equalize the
876 global contrast of the two stimuli. To assess the directional tuning of ROIs we used
877 full-field gratings drifting in 8 directions as above, with speeds 1500 or 1900 μm/s.
878
879 *Electrophysiology data analysis.* Numbers with errors quoted in the text are mean ±
880 standard error of the mean, unless otherwise specified. All data analysis was done
881 using custom written Matlab procedures. Individual peri-stimulus time histograms
882 (PSTH) presented for spikes, or current traces for voltage clamp recordings, were
883 averaged over three trials. Gray traces in Fig. 1B are individual trials. In population
884 response vs. speed data, curves from different cells were normalized by their
885 maximum and averaged. In population data where synaptic blockers or CNO were
886 used (DREADDs), the response curves for each cell were normalized by the maximum
887 of the control curve for that cell, and then curves were averaged over cells. The
888 currents presented for optogenetics (Fig. 4) were recorded at 20kHz, and in Fig. 4B-E
889 and 4J, current traces were averaged in 10ms windows. Current traces in Fig. 4 were
890 averaged over 3-5 trials. Direction and orientation selectivity indices (DSI, OSI) and
891 preferred directions and orientations were calculated from vector sums of responses
892 in different directions of motion [54,56].
893
894 *Immunohistochemistry*. Retinas were fixed and counterstained with the following
895 antibodies: Goat anti-ChAT (Choline acetyltransferase; 1:200, Millipore Sigma

896 #AB144); Rabbit anti VGluT3 (1:250, Invitrogen #PA5-85784). Chicken anti GFP
897 (1:1000, Abcam #ab13970) was used to enhance the fluorescence of the Cre-
898 dependent GFP virus. Rabbit anti-HA tag (1: 200, Cell Signaling Technology #3724)
899 was used to stain the HA-tagged hM4Di receptor in the VGluT3 x DREADD mouse.
900
901 *Imaging for cell targeting and dendritic morphology.* To target fluorescent cells for
902 patch recording, two photon imaging was used (Olympus FV1200MPE BASIC (BX-
903 61WI) microscope, 25×, 1.05 NA water-immersion objective (XLPL25XWMP,
904 Olympus), and an ultrafast pulsed laser (Mai Tai DeepSee HP, Spectra-Physics) tuned
905 to 910 nm. To acquire an image stack, RGCs were filled during electrophysiological
906 recordings with Alexa hydrazide 488 or 594 (100 μM, Invitrogen), and were imaged
907 following the recording, either using the two-photon or the single-photon (confocal)
908 configurations of the two-photon microscope. Tissue in which fluorescent proteins
909 were expressed was often fixed and immunostained (see above), and subsequently
910 imaged on a confocal microscope (Olympus FV3000, UPlan Super Apochromat
911 objectives, 30xS, 1.05 NA, or 60x2S, 1.3 NA) in the Leduc Imaging Facility, Brown
912 University. Confocal and two-photon stacks were processed in Fiji
913 (https://imagej.net/software/fiji), and collapsed using either maximum intensity or
914 maximum standard deviation projections.
915
916 *Functional imaging.* Imaging of calcium indicator signals were acquired using the
917 aforementioned two-photon microscope and conditions, as has been done previously
918 [54]. The frame rate was 15 Hz. For imaging responses in dendrites, 128 x 256 pixel

919 fields of view were used with a zoom of 4.5-5x (60 μm x120 μm FOVs). Light stimulus
920 presentation was synchronized to the fly-back times in the scanning of the
921 microscope so that they did not interfere with the measured signal.
922
923 *Functional imaging data analysis.* Functional imaging analysis was done using Fiji and
924 custom written Matlab routines. A standard deviation projection of movies were
925 made, over which ROIs were manually marked over brighter dendrites (Fig 6A), and
926 traces of their area-averaged brightness over time were acquired. For the baseline
927 fluorescence F_0, we averaged the brightness over 0.5 s before every stimulus
928 presentation. ROIs were chosen for analysis if their time averaged responses
929 surpassed a threshold $\Delta F/F_0$ (0.3 – 0.6) during at least 6 stimulus presentations out of
930 24. Fig. 6B-F show curves averaged over responsive ROIs.
931
932 *Intraocular injections.* Mice were anaesthetized with isoflurane (3% in oxygen; Matrx
933 VIP 3000, Midmark). A viral vector inducing Cre dependent expression of a payload
934 (see below) was injected into the vitreous humour of the right eye through a glass
935 pipette using a microinjector (Picospritzer III, Science Products GmbH). Analgesia
936 (Proparacaine, eye drops) was applied to the eye ~2 min before the injection, and
937 immediately following the injection (Buprenorphine SR, 0.02 ml, intraperitoneal) to
938 minimize postoperative pain. Mice were then taken off anesthesia, recovered within
939 several minutes, and monitored for 48 hrs following the procedure. Animals were
940 killed and retinas removed 14–21 d later.
941

942 *Viruses.* pAAV2/2-hSyn-DIO-hM4D(Gi)-mCherry (Addgene #44362, Roth Lab) was
943 injected intraocularly in VGluT3-Cre mice, causing Cre-dependent expression of
944 hM4D(Gi), a modified human muscarinic M4 receptor, that is an inhibitory Designer
945 Receptor Exclusively Activated by Designer Drugs (DREADD). AAV2/2-EF1a-DIO-
946 hChR2(H134R)-EYFP (from UNC vector core, Deisseroth Lab) was injected VGluT3-
947 Cre mice to express ChR2 in a Cre dependent manner, but mostly caused expression in
948 too few of the VGluT3 ACs to drive optogenetic responses in postsynaptic RGCs (Fig.
949 2E, Supp. Fig. 2D). rAAV2/2-CAG-flex-GFP (UNC vector core) was injected in Pcdh9-
950 Cre mice to target ON DSGCs for recording.
951
952 *Optogenetics.* Light stimulation to activate ChR2 was generated using a LED light
953 source (Mightex MLS-5500-MK1; LED driver: open-ephys.org, Cyclops) and
954 introduced through the microscope objective and GFP excitation filter cube, resulting
955 in a spectrum peak at 480±10 nm, and illumination over an area of 1 mm in diameter.
956 The light intensity at the sample was 0.9-1.4 nW/μm^2, the lowest intensity that
957 yielded robust postsynaptic responses in ON DSGCs. The stimulation time was 0.1 s or
958 1 s for 5 repeats, 4 s between repeats. The intensity and time were optimized for a
959 robust response, while minimizing the rundown of the response over time, and the
960 driving of large bursts of current that were sometimes observed, that were
961 inconsistent over trials or not stimulus-locked.
962
963 *Electron microscopy neuronal reconstructions.* An existing dataset of retinal sections
964 from a Serial Blockface Electron Microscope (SEM), 'k0725' [24] was used. The

965 imaged volume dimensions were 50 x 210 x 260 μm^3 with the short dimension
966 spanning the IPL and parts of the GCL and INL layers of the retina. The pixel size was
967 13.2 nm^2 and the section thickness 26 nm. The images contained intracellular details,
968 e.g. synaptic vesicles. The webKnossos platform (https://webknossos.org) was used
969 for tracing neuronal skeletons and annotating synapses . For the plot of stratification
970 depth (Fig. 3J), the depth of nodes in the skeletons were normalized to the depth of
971 the ON SAC plexus to correct for the tilt and curvature of the tissue in the block [57].
972

973 **Acknowledgements**

974 The authors are grateful to Roman Drabchuk for help in intraocular injections and
975 SEM cell tracing, to Rachel Gunderson for careful annotation of the Ca^{2+} imaging
976 movies, and to Dianne Boghossian for technical support. Supported by NIH R01
977 EY12973.
978

979 **References**

980 1. Simpson, J.I. (1984). The Accessory Optic System. Annu. Rev. Neurosci. *7*, 13–41.
981 2. Dhande, O.S., Estevez, M.E., Quattrochi, L.E., El-Danaf, R.N., Nguyen, P.L., Berson,
982 D.M., and Huberman, A.D. (2013). Genetic dissection of retinal inputs to
983 brainstem nuclei controlling image stabilization. J. Neurosci. *33*, 17797–17813.
984 3. Yonehara, K., Fiscella, M., Drinnenberg, A., Esposti, F., Trenholm, S., Krol, J.,
985 Franke, F., Scherf, B.G., Kusnyerik, A., Müller, J., *et al.* (2016). Congenital
986 Nystagmus Gene FRMD7 Is Necessary for Establishing a Neuronal Circuit
987 Asymmetry for Direction Selectivity. Neuron *89*, 177–193.

988 4. Goetz, J., Jessen, Z.F., Jacobi, A., Mani, A., Cooler, S., Greer, D., Kadri, S., Segal, J.,
989 Shekhar, K., Sanes, J., *et al.* (2021). Unified Classification of Mouse Retinal
990 Ganglion Cells Using Function, Morphology, and Gene Expression. SSRN
991 Electron. J., 1–27.
992 5. Sanes, J.R., and Masland, R.H. (2015). The Types of Retinal Ganglion Cells:
993 Current Status and Implications for Neuronal Classification. Annu. Rev.
994 Neurosci. *38*, 221–246.
995 6. Bae, J.A., Mu, S., Kim, J.S., Turner, N.L., Tartavull, I., Kemnitz, N., Jordan, C.S.,
996 Norton, A.D., Silversmith, W.M., Prentki, R., *et al.* (2018). Digital Museum of
997 Retinal Ganglion Cells with Dense Anatomy and Physiology. Cell *173*, 1293-
998 1306.e19.
999 7. Borst, A., and Euler, T. (2011). Seeing Things in Motion: Models, Circuits, and
1000 Mechanisms. Neuron *71*, 974–994. Available at:
1001 http://dx.doi.org/10.1016/j.neuron.2011.08.031.
1002 8. Oyster, C.W., Takahashi, E., and Collewijn, H. (1972). Direction-selective retinal
1003 ganglion cells and control of optokinetic nystagmus in the rabbit. Vision Res. *12*,
1004 183–193.
1005 9. Sivyer, B., Tomlinson, A., and Rowland Taylor, W. (2019). Simulated saccadic
1006 stimuli suppress ON-type direction-selective retinal ganglion cells via
1007 glycinergic inhibition. J. Neurosci. *39*, 4312–4322.
1008 10. Kay, J.N., de la Huerta, I., Kim, I.J., Zhang, Y., Yamagata, M., Chu, M.W., Meister, M.,
1009 and Sanes, J.R. (2011). Retinal ganglion cells with distinct directional
1010 preferences differ in molecular identity, structure, and central projections. J.

1011 Neurosci. *31*, 7753–7762.

1012 11. Barlow, H.B., and Levick, W.R. (1965). The mechanism of directionally selective
1013 units in rabbit's retina. J. Physiol. *178*, 477–504.

1014 12. Briggman, K.L., Helmstaedter, M., and Denk, W. (2011). Wiring specificity in the
1015 direction-selectivity circuit of the retina. Nature *471*, 183–190. Available at:
1016 http://dx.doi.org/10.1038/nature09818.

1017 13. Vaney, D.I., Sivyer, B., and Taylor, W.R. (2012). Direction selectivity in the
1018 retina: symmetry and asymmetry in structure and function. Nat. Rev. Neurosci.
1019 *13*, 194–208. Available at: https://doi.org/10.1038/nrn3165.

1020 14. Yonehara, K., Balint, K., Noda, M., Nagel, G., Bamberg, E., and Roska, B. (2011).
1021 Spatially asymmetric reorganization of inhibition establishes a motion-sensitive
1022 circuit. Nature *469*, 407–410. Available at:
1023 http://dx.doi.org/10.1038/nature09711.

1024 15. Matsumoto, A., Briggman, K.L., and Yonehara, K. (2019). Spatiotemporally
1025 Asymmetric Excitation Supports Mammalian Retinal Motion Sensitivity. Curr.
1026 Biol. *29*, 3277-3288.e5. Available at:
1027 https://doi.org/10.1016/j.cub.2019.08.048.

1028 16. Lee, S., Chen, L., Chen, M., Ye, M., Seal, R.P., and Zhou, J. (2014). An
1029 unconventional glutamatergic circuit in the retina formed by vGluT3 amacrine
1030 cells. Neuron *84*, 708–715. Available at:
1031 http://dx.doi.org/10.1016/j.neuron.2014.10.021.

1032 17. Grimes, W.N., Seal, R.P., Oesch, N., Edwards, R.H., and Diamond, J.S. (2011).
1033 Genetic targeting and physiological features of VGLUT3+ amacrine cells. Vis.

1034 Neurosci. *28*, 381–392.

1035 18. Haverkamp, S., and Wässle, H. (2004). Characterization of an Amacrine Cell
1036 Type of the Mammalian Retina Immunoreactive for Vesicular Glutamate
1037 Transporter 3. J. Comp. Neurol. *468*, 251–263.

1038 19. Johnson, J., Sherry, D.M., Liu, X., Fremeau, R.T., Seal, R.P., Edwards, R.H., and
1039 Copenhagen, D.R. (2004). Vesicular glutamate transporter 3 expression
1040 identifies glutamatergic amacrine cells in the rodent retina. J. Comp. Neurol.
1041 *477*, 386–398.

1042 20. Kim, T., Soto, F., and Kerschensteiner, D. (2015). An excitatory amacrine cell
1043 detects object motion and provides feature-selective input to ganglion cells in
1044 the mouse retina. Elife *4*, 1–13.

1045 21. Mani, A., and Schwartz, G.W. (2017). Circuit Mechanisms of a Retinal Ganglion
1046 Cell with Stimulus-Dependent Response Latency and Activation Beyond Its
1047 Dendrites. Curr. Biol. *27*, 471–482. Available at:
1048 http://dx.doi.org/10.1016/j.cub.2016.12.033.

1049 22. Heinze, L., Harvey, R.J., Haverkamp, S., and Wässle, H. (2007). Diversity of
1050 glycine receptors in the mouse retina: localization of the alpha4 subunit. J.
1051 Comp. Neurol. *500*, 693–707.

1052 23. Zhang, C., and McCall, M.A. (2012). Receptor targets of amacrine cells. Vis.
1053 Neurosci. *29*, 11–29.

1054 24. Ding, H., Smith, R.G., Poleg-Polsky, A., Diamond, J.S., and Briggman, K.L. (2016).
1055 Species-specific wiring for direction selectivity in the mammalian retina. Nature
1056 *535*, 105–110. Available at: http://dx.doi.org/10.1038/nature18609.

1057 25. Helmstaedter, M., Briggman, K.L., Turaga, S.C., Jain, V., Seung, H.S., and Denk, W.
1058 (2013). Connectomic reconstruction of the inner plexiform layer in the mouse
1059 retina. Nature *500*, 168–174. Available at:
1060 https://doi.org/10.1038/nature12346.
1061 26. Jain, V., Hanson, L., Sethuramanujam, S., Michaels, T., Gawley, J., Gregg, R.G., Pyle,
1062 I., Zhang, C., Smith, R.G., Berson, D., *et al.* (2022). Gain control by sparse, ultra-
1063 slow glycinergic synapses. Cell Rep. *38*, 110410. Available at:
1064 https://doi.org/10.1016/j.celrep.2022.110410.
1065 27. Della Santina, L., Kuo, S.P., Yoshimatsu, T., Okawa, H., Suzuki, S.C., Hoon, M.,
1066 Tsuboyama, K., Rieke, F., and Wong, R.O.L. (2016). Glutamatergic Monopolar
1067 Interneurons Provide a Novel Pathway of Excitation in the Mouse Retina. Curr.
1068 Biol. *26*, 2070–2077.
1069 28. Krishnaswamy, A., Yamagata, M., Duan, X., Hong, Y.K., and Sanes, J.R. (2015).
1070 Sidekick 2 directs formation of a retinal circuit that detects differential motion.
1071 Nature *524*, 466–470.
1072 29. Lee, S., Zhang, Y., Chen, M., and Zhou, Z.J. (2016). Segregated Glycine-Glutamate
1073 Co-transmission from vGluT3 Amacrine Cells to Contrast-Suppressed and
1074 Contrast-Enhanced Retinal Circuits. Neuron *90*, 27–34. Available at:
1075 http://dx.doi.org/10.1016/j.neuron.2016.02.023.
1076 30. Tien, N.W., Kim, T., and Kerschensteiner, D. (2016). Target-Specific Glycinergic
1077 Transmission from VGluT3-Expressing Amacrine Cells Shapes Suppressive
1078 Contrast Responses in the Retina. Cell Rep. *15*, 1369–1375. Available at:
1079 http://dx.doi.org/10.1016/j.celrep.2016.04.025.

1080 31. Lee, S., Chen, M., Shi, Y., and Zhou, Z.J. (2021). Selective glycinergic input from
1081 vGluT3 amacrine cells confers a suppressed-by-contrast trigger feature in a
1082 subtype of M1 ipRGCs in the mouse retina. J. Physiol. *0*, 1–14.
1083 32. Liu, J., and Sanes, J.R. (2017). Cellular and molecular analysis of dendritic
1084 morphogenesis in a retinal cell type that senses color contrast and ventral
1085 motion. J. Neurosci. *37*, 12247–12262.
1086 33. Rousso, D.L., Qiao, M., Kagan, R.D., Yamagata, M., Palmiter, R.D., and Sanes, J.R.
1087 (2016). Two Pairs of ON and OFF Retinal Ganglion Cells Are Defined by
1088 Intersectional Patterns of Transcription Factor Expression. Cell Rep. *15*, 1930–
1089 1944. Available at: http://dx.doi.org/10.1016/j.celrep.2016.04.069.
1090 34. Jacoby, J., and Schwartz, G.W. (2017). Three small-receptive-field ganglion cells
1091 in the mouse retina are distinctly tuned to size, speed, and object motion. J.
1092 Neurosci. *37*, 610–625.
1093 35. Schmidt, T.M., and Kofuji, P. (2009). Functional and Morphological Differences
1094 among Intrinsically Photosensitive Retinal Ganglion Cells. J. Neurosci. *29*, 476
1095 LP – 482. Available at: http://www.jneurosci.org/content/29/2/476.abstract.
1096 36. Stabio, M.E., Sabbah, S., Quattrochi, L.E., Ilardi, M.C., Fogerson, P.M., Leyrer, M.L.,
1097 Kim, M.T., Kim, I., Schiel, M., Renna, J.M., *et al.* (2018). The M5 Cell: A Color-
1098 Opponent Intrinsically Photosensitive Retinal Ganglion Cell. Neuron *97*, 150-
1099 163.e4. Available at: https://doi.org/10.1016/j.neuron.2017.11.030.
1100 37. Johnson, K.P., Zhao, L., and Kerschensteiner, D. (2018). A Pixel-Encoder Retinal
1101 Ganglion Cell with Spatially Offset Excitatory and Inhibitory Receptive Fields.
1102 Cell Rep. *22*, 1462–1472. Available at:

1103 https://doi.org/10.1016/j.celrep.2018.01.037.
1104 38. Jia, Y., Lee, S., Zhuo, Y., and Jimmy Zhou, Z. (2020). A retinal circuit for the
1105 suppressed-by-contrast receptive field of a polyaxonal amacrine cell. Proc. Natl.
1106 Acad. Sci. U. S. A. *117*, 9577–9583.
1107 39. Eggers, E.D., and Lukasiewicz, P.D. (2006). GABAA, GABAC and glycine receptor-
1108 mediated inhibition differentially affects light-evoked signalling from mouse
1109 retinal rod bipolar cells. J. Physiol. *572*, 215–225.
1110 40. Brüggen, B., Meyer, A., Boven, F., Weiler, R., and Dedek, K. (2015). Type 2 wide-
1111 field amacrine cells in TH:: GFP mice show a homogenous synapse distribution
1112 and contact small ganglion cells. Eur. J. Neurosci. *41*, 734–747.
1113 41. Park, S.J.H., Borghuis, B.G., Rahmani, P., Zeng, Q., Kim, I.J., and Demb, J.B. (2015).
1114 Function and circuitry of VIP+ interneurons in the mouse retina. J. Neurosci. *35*,
1115 10685–10700.
1116 42. Hsiang, J.C., Johnson, K.P., Madisen, L., Zeng, H., and Kerschensteiner, D. (2017).
1117 Local processing in neurites of VGluT3-expressing amacrine cells differentially
1118 organizes visual information. Elife *6*, 1–16.
1119 43. Rodieck, R.W. (1989). Starburst amacrine cells of the primate retina. J. Comp.
1120 Neurol. *285*, 18–37.
1121 44. Yamada, E.S., Dmitrieva, N., Keyser, K.T., Lindstrom, J.M., Hersh, L.B., and
1122 Marshak, D.W. (2003). Synaptic connections of starburst amacrine cells and
1123 localization of acetylcholine receptors in primate retinas. J. Comp. Neurol. *461*,
1124 76–90.
1125 45. Marshak, D.W., Chuang, A.Z., Dolino, D.M., Jacoby, R.A., Liu, W.S., Long, Y.,

1126 Sherman, M.B., Suh, J.M., Vila, A., and Mills, S.L. (2015). Synaptic connections of
1127 amacrine cells containing vesicular glutamate transporter 3 in baboon retinas.
1128 Vis. Neurosci. *32*.
1129 46. Jain, V., Hanson, L., Sethuramanujam, S., Gregg, R.G., Zhang, C., Smith, R.G.,
1130 Berson, D.M., McCall, M.A., and Awatramani, G.B. (2021). Gain control by sparse,
1131 ultra-slow glycinergic synapses. bioarxiv *1*, 1–42.
1132 47. Jacoby, J., and Schwartz, G.W. (2018). Typology and circuitry of suppressed-by-
1133 contrast retinal Ganglion cells. Front. Cell. Neurosci. *12*, 1–7.
1134 48. Tien, N.W., Pearson, J.T., Heller, C.R., Demas, J., and Kerschensteiner, D. (2015).
1135 Genetically identified suppressed-by-contrast retinal ganglion cells reliably
1136 signal self-generated visual stimuli. J. Neurosci. *35*, 10815–10820.
1137 49. Sabbah, S., Berg, D., Papendorp, C., Briggman, K.L., and Berson, D.M. (2017). A
1138 cre mouse line for probing irradiance- and direction-encoding retinal networks.
1139 eNeuro *4*, 1–21.
1140 50. Wienbar, S., and Schwartz, G.W. (2018). The dynamic receptive fields of retinal
1141 ganglion cells. Prog. Retin. Eye Res. *67*, 102–117. Available at:
1142 https://doi.org/10.1016/j.preteyeres.2018.06.003.
1143 51. Grimes, W.N., Schwartz, G.W., and Rieke, F. (2014). The synaptic and circuit
1144 mechanisms underlying a change in spatial encoding in the retina. Neuron *82*,
1145 460–473. Available at: http://dx.doi.org/10.1016/j.neuron.2014.02.037.
1146 52. Trenholm, S., Johnson, K., Li, X., Smith, R.G., and Awatramani, G.B. (2011).
1147 Parallel mechanisms encode direction in the retina. Neuron *71*, 683–694.
1148 Available at: http://dx.doi.org/10.1016/j.neuron.2011.06.020.

1149 53. Nath, A., and Schwartz, G.W. (2017). Electrical synapses convey orientation
1150 selectivity in the mouse retina. Nat. Commun. *8*. Available at:
1151 http://dx.doi.org/10.1038/s41467-017-01980-9.
1152 54. Sabbah, S., Gemmer, J.A., Bhatia-Lin, A., Manoff, G., Castro, G., Siegel, J.K., Jeffery,
1153 N., and Berson, D.M. (2017). A retinal code for motion along the gravitational
1154 and body axes. Nature *546*, 492–497. Available at:
1155 http://dx.doi.org/10.1038/nature22818.
1156 55. Wang, J., O'Sullivan, M.L., Mukherjee, D., Puñal, V.M., Farsiu, S., and Kay, J.N.
1157 (2017). Anatomy and spatial organization of Müller glia in mouse retina. J.
1158 Comp. Neurol. *525*, 1759–1777. Available at:
1159 https://pubmed.ncbi.nlm.nih.gov/27997986.
1160 56. Nath, A., and Schwartz, G.W. (2016). Cardinal orientation selectivity is
1161 represented by two distinct ganglion cell types in mouse retina. J. Neurosci. *36*,
1162 3208–3221.
1163 57. Sümbül, U., Song, S., McCulloch, K., Becker, M., Lin, B., Sanes, J.R., Masland, R.H.,
1164 and Seung, H.S. (2014). A genetic and computational approach to structurally
1165 classify neuronal types. Nat. Commun. *5*, 3512.
1166